TENSION-COMPRESSION FATIGUE BEHAVIOR OF 2D AND 3D POLYMER MATRIX COMPOSITES AT ELEVATED TEMPERATURE

THESIS

Saleh A. Alnatifat, Captain, RSAF

AFIT-ENY-MS-15-S-052

DEPARTMENT OF THE AIR FORCE
AIR UNIVERSITY

AIR FORCE INSTITUTE OF TECHNOLOGY

Wright-Patterson Air Force Base, Ohio

(IF your document is limited, place your Destruction Notice Here)

AFIT-ENY-12-M-05

TENSION-COMPRESSION FATIGUE BEHAVIOR OF 2D AND 3D POLYMER MATRIX COMPOSITES AT ELEVATED TEMPERATURE

THESIS

Presented to the Faculty

Department of Aeronautics and Astronautics

Graduate School of Engineering and Management

Air Force Institute of Technology

Air University

Air Education and Training Command

In Partial Fulfillment of the Requirements for the

Degree of Master of Science in Aeronautical Engineering

Saleh A. Alnatifat, B.S.M.E

Captain, RSAF

September 2015

AFIT-ENY-12-M-05

TENSION-COMPRESSION FATIGUE BEHAVIOR OF 2D AND 3D POLYMER MATRIX COMPOSITES AT ELEVATED TEMPERATURE

Saleh A. Alnatifat, B.S.M.E

Captain, RSAF

Committee Membership:

Dr. Marina B. Ruggles-Wrenn, PhD
Chair

Dr. Thomas G. Eason III, PhD
Member

Maj. Sheena Winder, PhD
Member

Abstract

The tension-compression fatigue behavior of the newly developed 3D and 2D polymer matrix composites (PMCs) was investigated. Additionally, the compressive stress-strain behavior and compressive properties of the two composites were evaluated. The two material systems studied tested in this effort consisted of a high-temperature polyimide NRPE matrix reinforced with carbon fibers. The 3D PMC was reinforced with carbon fibers in a non-crimp 3D orthogonal weave. The carbon fibers used in the 3D woven fabric were Grafil 34-700WD for the warp and fill fibers and AS4 for the Z fibers. The 2D PMC was reinforced with 15 plies of the 2D de-sized Cytec T650-35 carbon fibers woven in an eight harness satin weave. Compressive stress-strain behavior and compressive properties were evaluated at 23°C and at elevated temperature. Tension-compressive fatigue tests were performed at elevated temperature, with the ration of minimum to maximum stress of R = -1 at a frequency of 1 Hz. Fatigue run-out was set to 2×10^5 cycles. All specimens that achieved fatigue run-out were subjected to tension test to failure in order to evaluate the retained tensile properties. In all elevated temperature tests one side of the specimen was at 329°C and the other side was exposed to ambient air. Elevated temperature caused a decrease in compressive strength and modulus for both material systems. The 3D PMC exhibited a higher fatigue limit than the 2D PMC. However, at higher maximum stress levels the 2D PMC exhibited better fatigue performance than the 3D PMC. Examination of the failed specimens revealed significant

ply delamination in the 2D PMC, while the through-thickness Z-fibers restricted ply delamination in the 3D PMC.

Acknowledgments

First and foremost, I would like to thank Allah. I would also like to gratefully thank my advisor, Dr. Marina Ruggles-Wrenn, for her guidance and countless hours of support, not only during my thesis writing, but also through my master program and my injury recovery. In addition, I would like to extend my thanks to Capt. Michael Wilkinson (AFIT graduate) for his time and effort helping me during my training on the test machine. I would also like to thank Dr. Thomas Eason (AFRL/RQHF) and Dr. Sheena Winder (AFRL/RXAN) for their time and support. I would also like to thank the AFIT/ENY laboratory technicians Mr. Barry Page, Mr. Jamie Smith for their consistent support with lab equipments from training to maintaining. Thanks to my AFIT colleagues for making these two years, away from home, a wonderful and unforgettable experience.

A special thanks to my mother for her endless support, may Allah grant you a long happy life. Thanks to my brothers and sisters for your personal and moral support.

Last but not the least, Thanks to Mrs. Annette Robb for always being there for her international officers, the work you do and the endless support are not forgotten.

Table of Contents

Page

List of Figures

Page

List of Tables

Nomenclature

σ	Stress
E	Young's modulus (GPa)
R	$\frac{Minimum\ Stress}{Maximum\ Stress}$

List of Acronyms

2D	Two Dimensional
3D	Three Dimensional
AFIT	Air Force Institute of Technology
AFRL	Air Force Laboratory
HTPMC	High Temperature Polymer Matrix Composite
MS	Material System
MTS	Material System Test
PMC	Polymer Matrix Composite
Sic	Silicon Carbide
UCS	Ultimate Compressive Stress
UTS	Ultimate Tensile Stress

Tension-Compression Fatigue Behavior of 2D and 3D Polymer Matrix Composites At Elevated Temperature

I. Introduction

Advanced aerospace applications such as hypersonic vehicle airframes and aircraft engine components have raised demand for structural material systems that exhibit excellent thermal resistance, corrosion resistance and damage tolerance, as well as improved mechanical performance in elevated temperature environments. High-temperature polymer matrix composites (HTPMCs) are being considered for such applications. However, the polymer matrix in most HTPMCs cannot operate at temperatures required for many aerospace structural applications. Continuous research seeks to improve temperature capabilities of the HTPMCs, while also increasing their delamination resistance and impact resistance. It is recognized that delamination and impact resistance of a 2D woven composite can be improved by adding reinforcement through the thickness of the composite. The resulting non-crimp 3D woven composites have been demonstrated to exhibit improvements in delamination resistance, fracture toughness, damage tolerance, and impact performance [1].

An earlier study by Wilkinson [11] investigated mechanical properties and performance of two new HTPMCs developed by Polymer Performance Solutions Inc. ($P^2SI^{®}$) under contract with AFRL, a 2D weave PMC and 3D weave PMC. Wilkinson focused on tension-tension fatigue performance of these material systems at room and elevated temperatures. This research effort investigates tension-compression fatigue behavior of the aforementioned 2D and 3D material systems.

1.1 Motivation

Reduced life-cycle costs and increased aircraft availability are desirable for sustainment of current and future military aircraft. Material systems that show improved fatigue performance, excellent thermal resistance and damage tolerance, as well as resistance to corrosion and lightning strike are prime candidate materials for potential air vehicle structural components. Airframe structures and components on many existing and future Air Force systems reach elevated temperatures during operation. Examples include hypersonic vehicle airframes, engine related components (such as engine ducts, engine vanes, and exhaust flaps), and hot trailing edges of B-2 and C-17 wings. In the last three decades application of advance composite materials in military aircraft structure have grown tremendously due to their property of high strength to weight ratio, those advanced composite materials are being extensively researched and studied. As an example of the growth of using composite materials for US fighter aircraft structure Figure 1 shows the usage percentage of three different aircrafts [10].

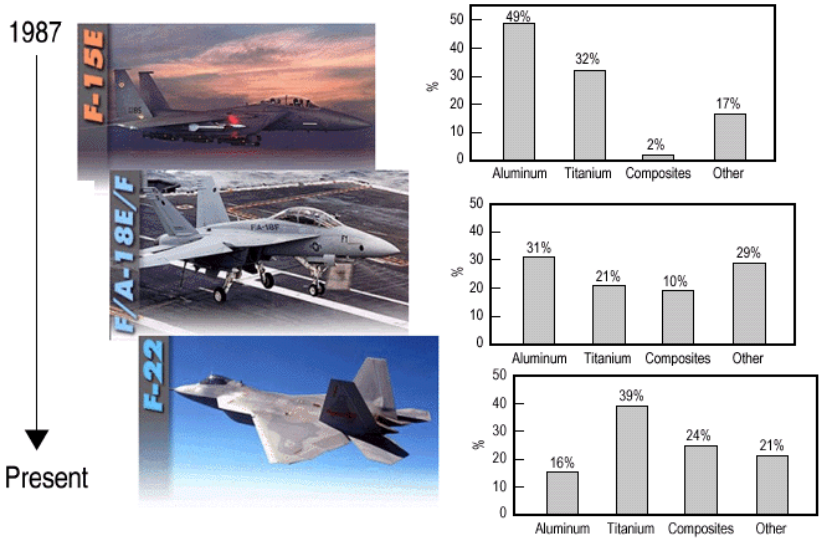

Figure 1: Materials usage trends in US aircraft. Reproduced from [10].

Many aircraft industries use Polymer Matrix Composites (PMCs) and Ceramic Matrix Composites (CMCs) for structure that is subjected to high temperature. While PMR-15 being the most widely used as a thermosetting polyimide resins for high-temperature polymer matrix composites (HTPMCs) applications, other polyimide resins replacement are being researched and developed due to the carcinogenic elements in the PMR-15 [6]. Performance Polymer Solutions Inc. ($P^2SI^{®}$) has been developing NRPE polyimide. A two-dimensional (2D) weave and three-dimensional (3D) weave of carbon-reinforced NRPE-matrix composites have been fabricated for the Air Force Research Laboratory (AFRL).

Before these newly-developed material systems can be reliably used in aircraft structural applications, their structural integrity and environmental durability must be assured. It is necessary to gain fundamental understanding of the structural performance of these material systems under static and cyclic loadings histories at elevated temperature.

1.2 Problem Statement

Aircraft industries favors using PMC's over conventional metal for structure components in applications where high strength is required with a weight savings, where the glass transition temperature of the matrix constituent of HTPMCs can be exceeded in many of those structural components. This leads to the necessity of developing new materials or using thermal protection material systems to enable those PMCs to operate in these harsh environments. Also, the mechanical properties of those new material systems should be studied and experimentally investigated in simulated operational environments

in order to verify their ability to endure complex loading during high temperature applications.

1.3 Research Objectives

The objective of this research is to characterize compression properties and to investigate tension-compression fatigue performance of two newly-developed composite systems at room and elevated temperature. The material systems investigated in this research were:

MS1: PMC with 3D woven fibers

MS2: PMC with 2D woven fibers

The present research effort builds on prior work by Wilkinson [11], who evaluated tensile properties and assessed tension-tension fatigue behavior of these material systems at room and elevated temperature.

1.4 Methodology

The following tasks were accomplished to achieve the thesis objective:

1. Perform monotonic compression to failure tests at room and elevated temperature to characterize compression properties and stress-strain behavior of the 2D and 3D PMCs with 0/90° fiber orientation.
2. Perform tension-compression fatigue tests at elevated temperature for both material systems and analyze experimental results.
3. Examine the fracture surfaces using an optical microscope in order to evaluate damage and failure mechanisms.

II. Literature Review

2.1 Composite Materials

A composite material consists of two or more materials forming a material with better properties than the properties of each constituent material alone. Reinforcement and matrix comprise the basic structure of a composite material. Being harder, stronger, and stiffer in most cases the reinforcement phase provides the strength and stiffness for the composite material. The reinforcement can be a fibers, whiskers or particulate. Glass, aramid and carbon are typically used as fibers that could be continuous or discontinuous.

On the other hand the matrix phase is continuous and comes as polymer, metal or ceramic. Among many purposes the matrix phase supports the fibers and bonds them together. Also, it transfers shear loads to the fibers [4]. In composite materials, the arrangement of fibers (as unidirectional or woven) in a matrix is called laminae. A material that consists of more than one laminae is known as laminate. These piles of laminae are bonded together with different orientations of fibers directions in each laminae [12]. Figure 2 shows a view of laminate construction.

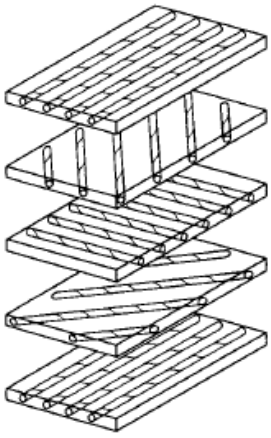

Figure 2: Un-bonded View of Laminate Construction. Reproduced from [12].

By changing the number of lamiae, a laminate composite can be produced with different thicknesses. Delamination, or in other term interlaminar separation, occurs in laminate composite. Through the failure process this delamination can interact with transverse cracking [3].

2.2 Polymer Matrix Composites

Thermoset and thermoplastic are the two matrix categories in PMCs. Thermosetting resins can be polyesters, vinyl-esters, epoxies, and polyamides. Curing process in thermoset resins occur when they experience chemical reactions which crosslink the polymer chains in a three dimensional network. As a result they gain a high dimensional stability and high temperature resistance. Thermoplastic resins (or engineering plastics) can be polyesters, poly-etherimide, polyamide imide, polyphenylene sulfide, polyether-etherketone (PEEK), and liquid crystal polymers. The processing of the thermoplastics is reversible unlike the curing process of thermosetting resins. Figure 3 below shows the overall characteristics of each matrix type [16].

Resin type	Process temperature	Process time	Use temperature	Solvent resistance	Toughness
Thermoset	Low	High	High	High	Low
Toughened thermoset	↑	↓	↑	↑	↓
Lightly crosslinked thermoplastic	↑	↓	↑	↑	↓
Thermoplastic	High	Low	Low	Low	High

SOURCE: Darrel R. Tenney, NASA Langley Research Center.

Figure 3: comparison of general characteristics of thermosets and thermoplastics. Reproduced from [16]

Glass, carbon, silicon carbide (SiC), and aramid are usually used as reinforcement material in PMCs [2]. Material systems studied in this research utilize carbon fibers.

One important aspect of composite materials construction is the interface region between the matrix and the fibers. The stronger bond is better for load behavior in PMCs. In contrast, a weak bond is preferable for CMCs to avoid brittle failure and help to achieve crack deflection around fibers [2].

2.3 Composite Compression and Fatigue Response

Figure 4 shows a schematic of a composite stress-strain behavior under monotonic loading. Stress-strain behaviors of the composite constituents (i. e. fibers and matrix) are also included. Note that Figure 4 shows stress magnitude plotted vs. strain magnitude. The slope of the linear range of stress-strain curve is called compressive modulus, E_C, which is a measure of material stiffness. In compression the lowest stress value that the material could sustain is called the ultimate compression stress.

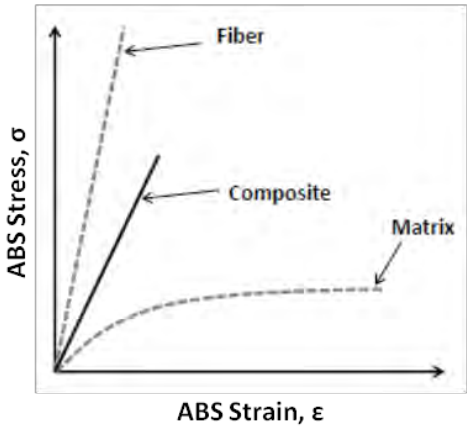

Figure 4: Illustrative compression stress-strain curve.

Fatigue experiments are performed to evaluate the material behavior under cyclic loading. Experimental results are frequently represented by plotting maximum stress vs. cycles to failure or the S-N curve (see Figure 5).

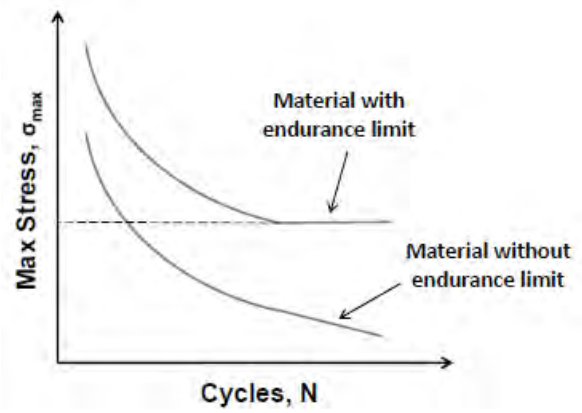

Figure 5: Example of S-N curve.

2.4 Composite Weave Patterns

A 2D weaving process uses 2 sets of yarns that are perpendicular to each other called the warps and the wefts. The warps run in the longitudinal direction of the fabric, where the wefts run in the transverse direction [15].

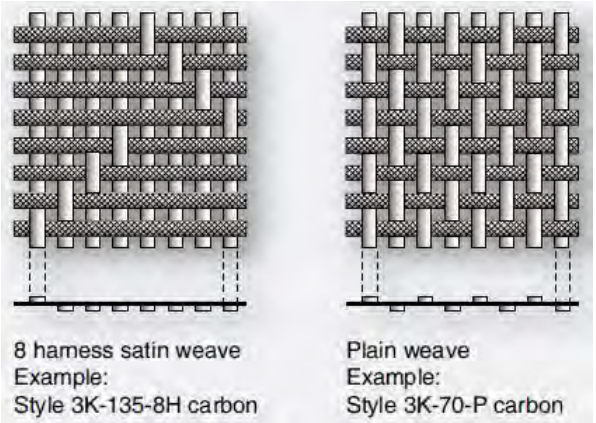

Figure 6: Examples of fabric weave styles. Reproduced from [5].

Another weaving process is being researched and developed to enhance the strength in the through-thickness direction of the composite and help prevent ply delamination, see Figure 7. This 3D weaving process uses an extra set of weft yarns in the vertical direction perpendicular to the 2 sets of yarns used to form the 2D PMC or CMC. The intention is to add higher strength and stiffness in Z direction of the composite. However, this addition of z fiber direction in most cases results in lower in-plane strength and modulus [15].

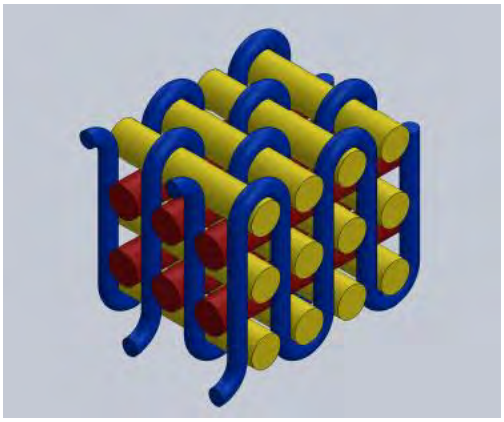

Figure 7: Representation of non-crimp 3D orthogonal weave. Warp yarns in red, weft yarns in yellow and Z yarns in blue.

2.5 Previous Research

Numerous researchers have investigated mechanical behavior of PMC materials with similar constituents, for example PMR-15/carbon fiber composites. Recently Wilkinson [11] evaluated tensile properties and studied tension-tension fatigue behavior of the 2D and 3D PMCs investigated in this work. Results obtained by Wilkinson in

tension-to-failure tests are summarized in Tables 1 and 2. Wilkinson observed that, the 2D PMC has a higher ultimate tensile strength and stiffness than of those obtained for the 3D PMC at room and elevated temperature. Also, the tensile properties of both the 2D and 3D PMCs were little affected by the increase of the temperature.

Table 1: Summary of tensile properties for 3D PMC 0/90° at room temperature and elevated temperature (329°C). Data from Wilkinson [11].

Fiber oriantation	Specimen #	Temperature (°C)	Elastic Modulus (GPa)	Normalized Modulus (GPa)	UTS (MPa)	Normalized UTS (MPa)	Failure Strain (%)
[0/90]	T3-1	23 / 23	39.99	47.17	699.3	824.9	1.645
	T3-3	23 / 23	52.31	48.42	772.9	715.5	1.172
	T3-5	23 / 23	41.46	46.31	713.8	797.2	1.644
	Room Temp Average:		**44.59**	**47.30**	**728.7**	**779.2**	**1.487**
	T3-2	173 / 329	48.40	46.65	762.5	734.9	1.407
	T3-4	154 / 329	47.44	49.53	746.4	779.3	1.405
	T3-6	165 / 329	41.30	45.66	681.9	753.9	1.602
	Elev Temp Average:		**45.71**	**47.28**	**730.3**	**756.0**	**1.472**

Table 2: Summary of tensile properties for 2D PMC 0/90° at room temperature and elevated temperature (329°C). Data from Wilkinson [11].

Fiber oriantation	Specimen #	Temperature (°C)	Elastic Modulus (GPa)	Normalized Modulus (GPa)	UTS (MPa)	Normalized UTS (MPa)	Failure Strain (%)
[0/90]	T1-1	23 / 23	56.87	57.29	831.8	837.9	1.401
	Room Temp Average:		**56.87**	**57.29**	**831.8**	**837.9**	**1.401**
	T1-2	158 / 329	60.93	61.88	834.4	847.3	1.276
	T1-6	139 / 329	59.04	58.03	809.6	795.7	1.287
	Elev Temp Average:		**59.99**	**59.95**	**822.0**	**821.5**	**1.281**

Results obtained for the 2D and 3D PMCS by Wilkinson in tension-tension fatigue tests are summarized in Tables 3 and 4. Wilkinson found that, the 2D PMC has a better tension-tension fatigue performance than the 3D PMC tension-tension fatigue performance. In the other hand, the 3D PMC offers improved delamination resistance.

Table 3: Tension-tension fatigue results for 3D PMC 0/90° at elevated temperature (329°C). Data from Wilkinson [11].

Specimen #	Maximum Stress (MPa)	Maximum Stress (% UTS)	Normalized Max. Stress (MPa)	Normalized Max. Stress (% UTS)	Cycles to Failure (N)	Failure Strain (%)	Modulus Loss (%)
T3-18	621.2	85	661.0	87	1,159	0.255	-7.901
T3-17	643.0	88	640.0	85	519	0.051	-61.543
T3-15	621.7	85	609.9	81	10,141	0.258	1.229
T3-19	623.0	85	592.9	78	57,373	0.275	7.005
T3-11	584.8	80	575.1	76	75	0.089	-1.754
T3-14	563.4	77	558.4	74	85,931	0.366	30.410
T3-12	549.4	75	551.0	73	159,828	0.091	16.968
T3-13	512.5	70	528.7	70	167,979	0.232	25.841
T3-8	586.4	80	526.0	70	45,091	0.015	22.638
T3-9	513.8	70	518.0	69	150,741	0.453	61.187
T3-10	476.0	65	482.9	64	200,000	0.122	-0.422
T3-7	440.9	60	424.7	56	200,000	0.047	8.232

Table 4: Tension-tension fatigue results for 2D PMC 0/90° at elevated temperature (329°C). Data from Wilkinson [11].

Specimen #	Maximum Stress (MPa)	Maximum Stress (% UTS)	Normalized Max. Stress (MPa)	Normalized Max. Stress (% UTS)	Cycles to Failure (N)	Failure Strain (%)	Modulus Loss (%)
T1-5	740.1	90	759.7	92	2,756	0.130	5.392
T1-12	740.8	90	734.3	89	1,148	1.649	28.813
T1-11	723.9	88	719.8	88	10,916	bad	bad
T1-8	699.6	85	683.7	83	11,286	0.308	14.035
T1-3	658.0	80	663.0	81	23,768	1.111	23.849
T1-10	618.4	75	610.2	74	121,136	0.787	66.281
T1-7	576.3	70	585.3	71	200,000	0.057	20.430
T1-4	494.5	60	503.3	61	200,000	0.167	5.141

III. Materials and Test Specimens

This section provides a description of the material systems investigated in this research. Also, test specimen geometry used and test specimen preparation are discussed.

3.1 Material System 1 (MS1): 3D Weave PMC

The material system MS1 consists of a polymer matrix reinforced with carbon fibers in a three dimensional woven fabric pattern. The matrix material is a high temperature PMR-type polyimide resin called NRPE. NRPE shows low melt viscosity compared to PMR-15 and retains its mechanical properties at temperatures up 343˚C [9]

Table 5, provided by P^{2}SI® shows the 3D fabric design of the MS1. The structure of the 3D weave is composed of Z-direction yarns that interweave warp yarns with multiple insertions of fill yarns in the transverse direction. The carbon fibers used for the warp and fill fibers are Grafil 34-700WD and AS4 for the Z fibers. In this 3D weave the fabric pattern is non-crimp weave. Resin film infusion method is used to manufacture this material system.

Table 5: Three-dimensional fabric design with property predictions. Data from manufacturer

# Warps	Warp Tow	dpi[1]	# Fills	Fill Tow	ppi[2]	Z Tow	% of Warps	% of Fills	% of Z	h, mm	V_f, %
4	24K	8	5	12K	6.5	3K	47.9	48.6	3.5	4.9	58.1

[1] *dents per inch (dent - space between the wires of a reed on a loom through which the warp yarns pass)*
[2] *picks per inch (pick - single fiber fill yarn pulled through a weave)*

3.2 Material System2 (MS2): 2D Weave PMC

The MS2 consists of the NRPE polymer matrix reinforced with carbon fibers in a 2D woven fabric pattern. The MS2 is reinforced with 15 plies of 2D carbon de-sized Cytec T650-35 fibers interlaced in an 8 harness satin weave. Manufacturer used prepreg method to fabricate this material system. Refer to Table 6 for panel properties (MS2-1).

Table 6: PMC panels constituent properties. Data from manufacturer.

	Resin Content	Fiber Volume Fraction	Resin Volume Fraction	Void Volume Fraction	Density (g/cc)
MS1-1	39.10%	52.87%	45.26%	1.87%	1.563
MS2-1	36.44%	55.29%	42.26%	2.45%	1.566

3.3 Specimen Geometry

Tension-compression fatigue specimens studied in this research were machined from the same panels as the tension-tension fatigue specimens of the same fiber architecture. Because compressive loading, and thus the potential for buckling failure modes, is involved in the tension-compression cycle, specimens with hourglass-shaped gage section (Figure 8) were used in all tests. The stress concentration inherent in an hourglass-shaped specimen was assessed. Finite element analysis of the specimen shows that the axial stress at the edges in the middle of the hourglass section is only 3.5% higher than the average axial stress. Recently, specimens with an hourglass-shaped gage section have been successfully used in tension-compression fatigue tests of glass strand composites and SiC/SiC composites to minimize potential buckling in compression [7].

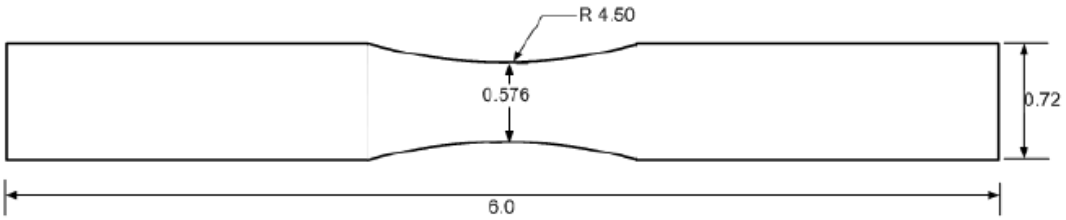

Figure 8: Tension-compression specimen geometry. All dimension in inches.

3.4 Specimen Preparation

The AFIT Model and Fabrication shop used diamond-grinding to machine test specimens from composite panels. The test specimens of the two material systems studied in this research were cut with 0/90° fiber orientation. Then each specimen was labeled. The specimen labels refer to specimen geometry, material system and fiber orientation. For instance, C1-3 refers to tension-compression specimen number 1 with 0/90° fiber orientation cut from a panel of the 2D PMC (panel MS2-1). See Table 7 for more details.

Table 7: Specimen labeling scheme

Material System	Material Type/ Fiber Weave	Panel ID	Fiber Orientation	Label	Example Specimen Labels	Number of Specimens
MS1	3D PMC	MS1-1	0/90	C3	C3-1	11
MS2	2D PMC	MS2-1	0/90	C1	C1-3	10

Width and thickness were measured in the gage section of each specimen using Mitutoyo Absolute Solar Digimatic Caliper, Model NO. CD-S6”CT. The measurements were performed and reported by Wilkinson [11]. Table 8 Lists average test specimen dimensions

Table 8: Average tension-compression specimen dimensions. Data from Wilkinson [11].

Material System	Panel	Specimen Type	Average Width (mm)	Average Thickness (mm)	Avg Cross-Sect. Area (mm^2)
1	1	3D [0/90] PMC	14.6376	4.7121	68.9771
2	1	2D [0/90] PMC	14.6427	5.7285	83.8798

All specimens were washed with soap and water, and rinsed with purified water in order to remove contamination from the machining process contamination. Specimens were then dried in an Isotemp Model 282A vacuum oven at 105°C with nearly 2 inches Hg pressure. To assess moisture desorption, weight measurements were noted for four specimens of each type on a periodic basis using a Mettler Toledo laboratory balance accurate to ± 0.9 mg. After the specimen weight has stabilized, specimens were removed from the oven and kept in a desiccator until testing. Specimen weight loss vs. drying time is shown in Figure. 9.

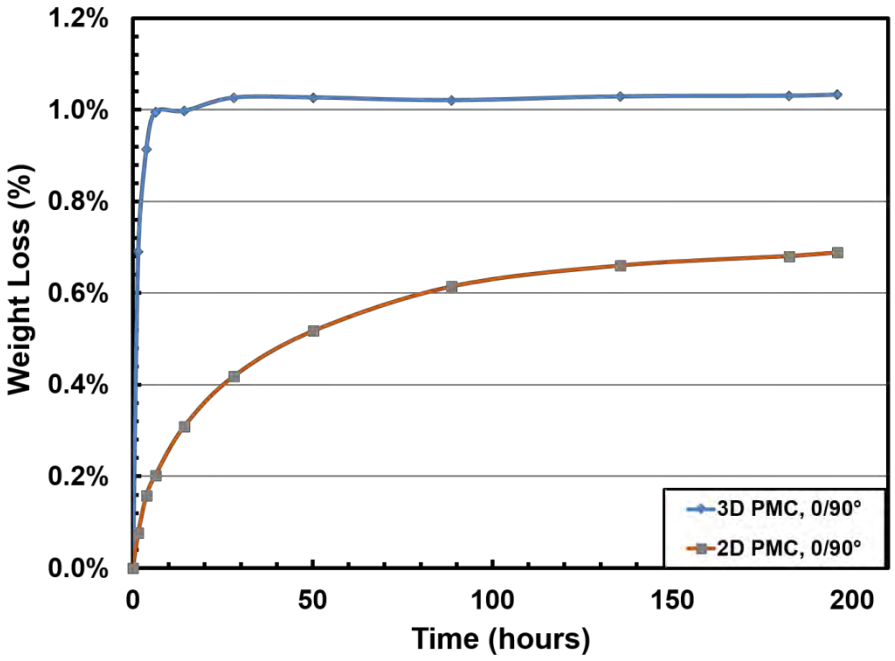

Figure 9: Specimen weight loss over time. Reproduced from Wilkinson [11].

In the side of the test specimen two dimples were prepared to keep the axial extensometer in position during the tests. Dimples were made with a minimal depth to avoid failure initiation at the dimples.

Fiberglass tabs were attached to the top and bottom surfaces of the specimen with tape in order to prevent the wedge surface from damaging the specimen and to transfer the load to the specimen during initial modulus tests. For all other tests, the tabs were attached to the specimen grip area with M-bond 200. A fiberglass tab of $^{1}/_{16}$'' thickness was used. See Figure 10.

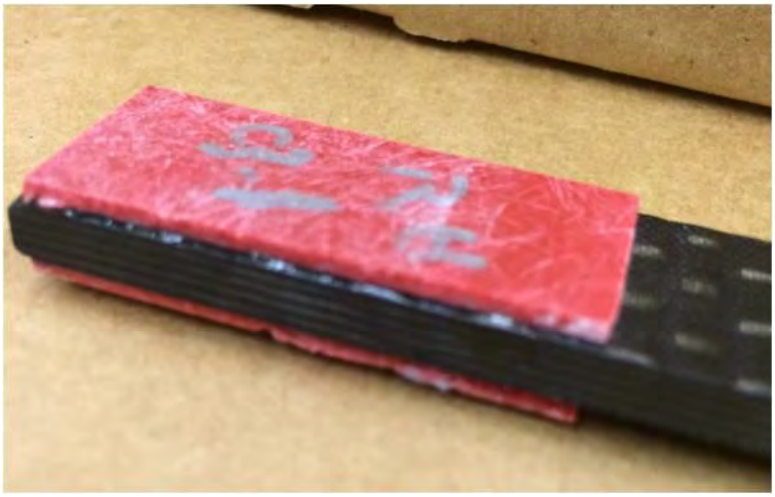

Figure 10: specimen with grip tap installed.

IV Experimental Setup and Test Procedures

This section provides a description of the test equipment and setup, temperature calibrations, tests procedures and optical microscopy used in this research.

4.1 Mechanical Testing Equipment

A Model 810 MTS servo-hydraulic testing machine equipped with a 100 kN (22 kip) configured model 647.10A load cell were used for the room temperature modulus calculations. MTS model 647.10 water-cooled hydraulic wedge grips had a grip pressure of 5 MPa. Strain measurements were obtained with MTS model 632.53E-14 axial extensometer with a 12.7-mm gage section.

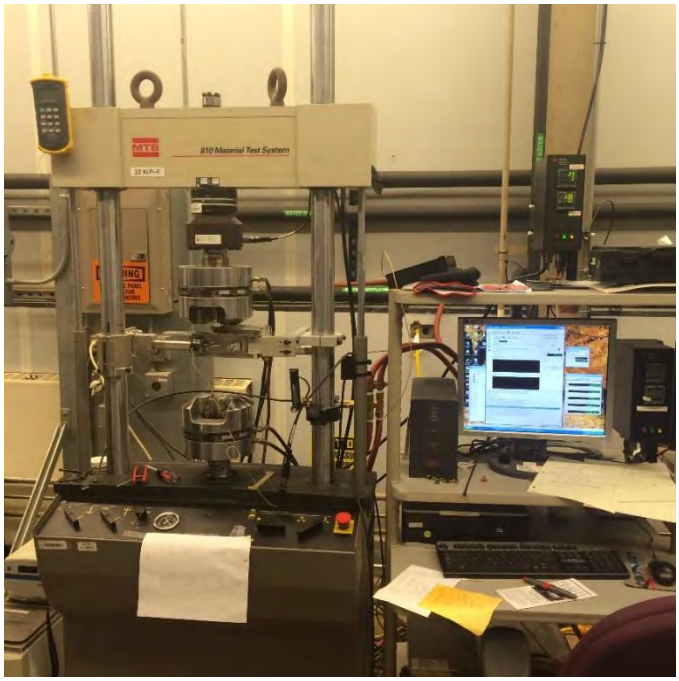

Figure 11: Overview of the test station.

The same testing machine detailed above was used to perform all other room and elevated temperature tests. In case of elevated temperature tests, a single zone MTS 653 furnace connected to an MTS 409.83 temperature controller was used. The grip pressure

varied from material system to another. A 15 MPa grip pressure was used in all 2D specimens test for the monotonic compression to failure and the tension-compression fatigue tests. The 3D specimens' tests performed with a lower grip pressure to avoid specimen grip section crushing. Figure 12 depicts the 22 kip hydraulic testing machine, furnace and extensometer.

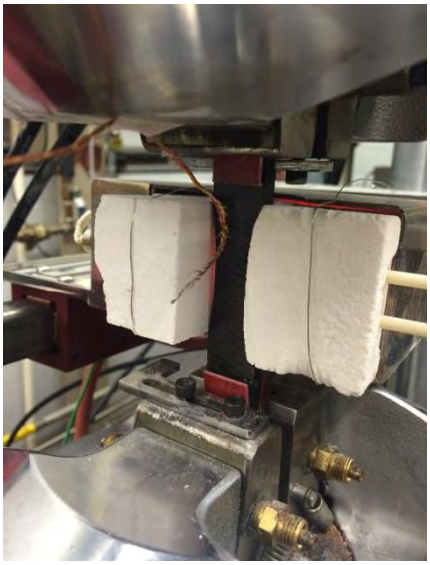

Figure 12: Close up view of the test setup.

Data acquisition and input signal generation were accomplished using a Flex Test 40 digital controller. MTS station builder release 5.2B was used to generate a configuration, where the station manager interface was used to perform operations. Different procedures were developed to run different type of tests and collect desired data as well. For each test these following data were collected: force, force command, displacement, strain, right temperature, and time.

4.2 Temperature Calibration

For each material system a temperature calibration was carried out to keep the side of the specimen facing the furnace at a temperature of 329° C. Before conducting the temperature calibration procedure, the specimen was prepared by attaching two type K thermocouples, one on the face facing the furnace, and one the other side open to ambient air. First the thermocouples were placed at the center of the specimen gage and a Kapton tape was wrapped around the specimen, and then secured with Nickel Chromium wire see Figure 13. A temperature sensor of a type Omega HH501DK was used to read the temperature on the side of the specimen. The shiny surface of both material systems was installed facing the ambient air to be consistent with Wilkinson research [11].

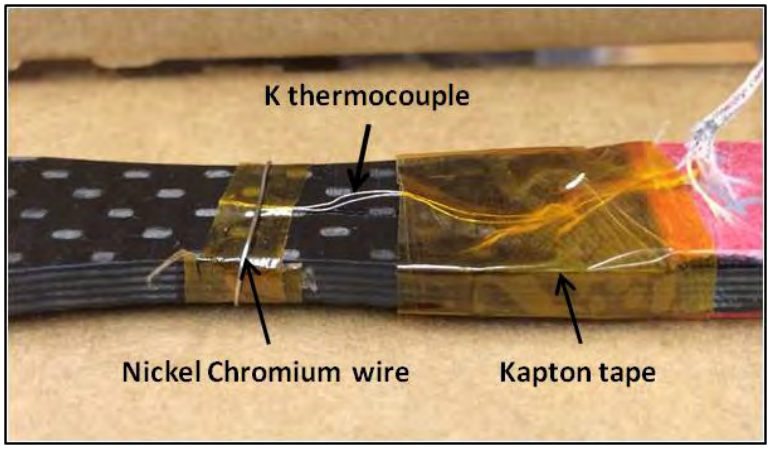

Figure 13: Temperature calibration specimen.

The one side heating objective was achieved by shaping the furnace insulation inserts to be consistent with the specimen geometry. This effort will help to direct the furnace heat to one side and keep the other side of specimen open to ambient air. The main piece of the inserts was carved to fit inside the furnace with enough holes in the

middle to allow the heat of the furnace reach the gage center on the side of the specimen. Then another block of the insert was tied to the furnace with a wire behind the back side of the specimen. After the specimen was installed in testing machine another hollow insulation piece was placed against the furnace and around the extensometer and tied with a wire.

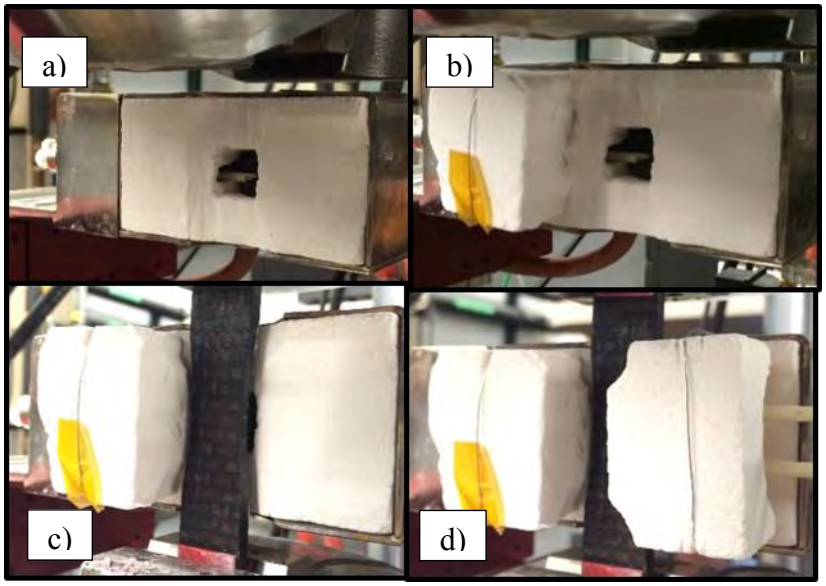

Figure 14: Furnace insulation setup: a) Inside furnace insert b) Specimen back side insert c) Specimen gripped d) Specimen front side insert

A temperature calibration procedure was developed using MTS software, to ramp the furnace temperature, using the temperature controller, to a set point with a rate of 10°C/min. When the furnace temperature reached the set point, then the furnace temperature was adjusted manually until the temperature of the right side of the specimen T_{right}, was at 329°C. This setting was then kept for a 3 hours to make sure that T_{right} stayed at 329°C with a ±5°C margin of error. This temperature calibration was done for both of material systems. The furnace insulation insert were destroyed during a 3D specimen test,

with two specimens left untested. A new furnace insulation insert was craved to fit the furnace. Then another temperature calibration was conducted for the remaining 3D specimens. During the actual tests, the temperature readings of the unheated side varied from specimen to specimen. This variability could have been a result of multiple reasons. One was the insulation was not in the same place each time a new specimen was tested. Another reason could have been due to changes in the laboratory ambient air temperature. Also, furnace position relative to the specimen might contribute to the variability of the temperature. The furnace set point temperature for each material system is shown in Table 9.

Table 9: Furnace set point temperature for elevated temperature tests

Specimen Type	Furnace Set-point °C
3D PMC	552 / 446
2D PMC	446

4.3 Mechanical Test Procedures

4.3.1 Room Temperature Elastic Modulus Measurements.

For each specimen the room temperature elastic modulus was measured to assess specimen to specimen and panel to panel variability. These modulus tests were carried out prior to any other tests. The specimens were loaded to 20 MPa stress in a stress control mode at a rate of 1 MPa/s, then brought to a zero load stress at the same rate. This process was repeated three times to get an average modulus from the load and unload

segments. The modulus was obtained by taking the slope of the best fit line on a stress-strain curve for each segment. This work was performed by Wilkinson [11].

4.3.2 Monotonic Compression Tests.

As stated in the objective earlier, monotonic compression-to-failure test we performed at room temperature and elevated temperature. The room temperature test was carried out to evaluate as-processed mechanical properties of the material systems. Then the same test was carried out with the right side of the specimen at an elevated temperature of 329°C. One specimen from each material system was tested at room temperature, while two specimens from each material system were tested at elevated temperature.

MTS software was used to create the test procedures where the specimen was loaded in displacement control at a rate of 0.025 mm/s. Failure was considered when a dramatic drop in the load occurred. For the elevated temperature tests, the temperature controller was used to ramp the furnace temperature to the set point at a rate of 10°C/min and then kept constant for 45 min prior loading the specimen in displacement control to failure. The data acquisition for these tests included force, displacement, displacement command, strain, temperature, temperature command and time.

4.3.3 Fatigue Tests.

All the tension-compression fatigue tests were carried out at an elevated temperature where T_{right} is 329°C with a stress ratio of R = -1 and frequency of 1 Hz. Fatigue performance of each material system was evaluated at different maximum stress levels. Fatigue run-out was defined as 2×10^5 cycles. All specimens that achieved fatigue

run-out were tested in tension to failure at elevated temperature to evaluate the retained tensile properties. In the tension-to-failure tests the specimen was loaded in displacement control at a rate of 0.025 mm/s. Failure was considered when a dramatic drop in the load occurred.

The test procedure was created using the MTS software. First, the temperature controller would ramp the furnace temperature to the set point determined during temperature calibration at a rate of 10°C/min. Then the temperature was kept constant during the test progress. After 45 min soak at temperature, the procedure would start the cyclic loading using a sine waveform in force control. The procedure would stop if the specimen failed before reaching run-out ($2x10^5$). If failure did not occur, the procedure would stop the cyclic loading and then proceed to the tension-to-failure tese to assess the retained properties of the specimen in comparison to the specimen properties before cyclic fatigue loading.

To be consistent with prior work [11, p. 37] the following test procedure and data acquisition scheme were used in this research:

- Warm-up: for the temperature ramp up and 45 min dwell period: data collected every 15 seconds and saved to the *specimen* data file.
- Fatigue:
  - Collect Peak & Valley Data: for each cycle the data at the maximum and minimum points were collected and saved to *Peak_Valley* data file.
  - Collect Cyclic Data: for selected number of cycles (specified below) the data was collected every 0.01 seconds and saved to *Cyclic* data file.

- Cycles 1-25
- Every 10th cycle from 30 to 100
- Every 100th cycle from 100 to 1000
- Every 1,000th cycle from 1,000 to 10,000
- Every 10,000 cycle from 10,000 to 200,000

- Tension to Failure: data collected every 0.01 seconds and saved to *Tension_to_failure* data file.

4.4 Optical Microscopy

After testing, all specimens were examined under a Zeiss Discovery V12 stereoscopic optical microscope equipped with a Zeiss AxioCam HRc digital camera. Examination via optical microscope facilitates determination of failure mechanism.

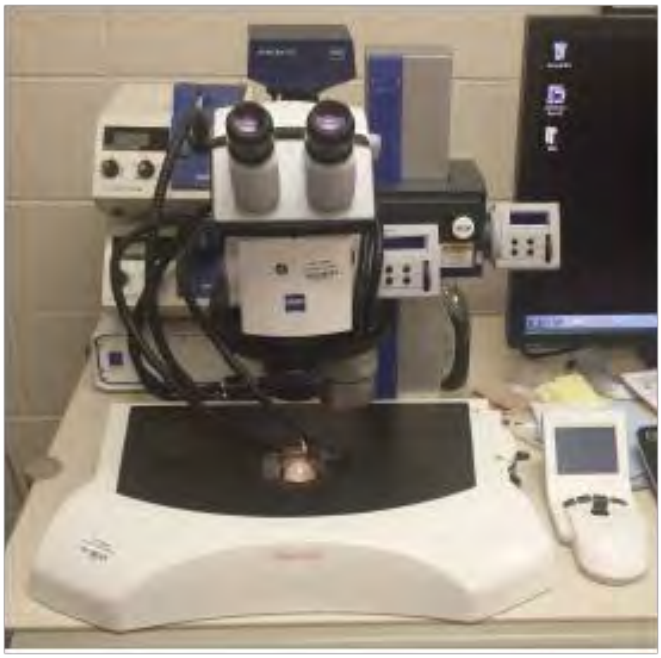

Figure 15: Zeiss optical microscope.

V. Results and Discussions

5.1 Assessment of Specimen-to-Specimen Variability

A slight defect in the processing and manufacturing of a composite panel could lead to variability in mechanical properties. Consequently, an assessment of the specimen-to-specimen variability was essential. In order to assess specimen-to-specimen and panel-to-panel variability, elastic modulus of each test specimen was measured at room temperature. The average room-temperature modulus values reported by Wilkinson [11] are presented in Table 10.

Table 10: Room temperature elastic modulus results for tension-compression specimens. Data from Wilkinson [11].

Panel	Specimen Type	Average Modulus (GPa)	Standard Deviation (GPa)	Coeff. Of Variation
MS2-1	C1: [0/90] 2D-PMC	52.1112	1.8081	0.0347
MS1-1	C3: [0/90] 3D-PMC	40.0783	4.0316	0.1006

The modulus of the 0/90° 2D PMC specimens was consistently greater than that of the 0/90° 3D PMC specimens. Also, it was observed that 3D PMC specimen exhibited greater variability in the modulus values. This could have been due to the addition of the Z fibers which required a complex processing that could result in more defects in the final product. The modulus values obtained for tension-tension specimens are shown in Table 11.

Table 11: Room temperature elastic modulus results for tension-tension specimens. Data from Wilkinson [11].

Panel	Specimen Type	Average Modulus (GPa)	Standard Deviation (GPa)	Coeff. of Variation
MS2-1	T1: 2D PMC, [0/90]	59.0076	1.4738	0.0250
MS1-1	T3: 3D PMC, [0/90]	46.4654	3.4979	0.0753

The comparison between the initial modulus values obtained for tension-tension and tension-compression specimens at room temperature revealed a slight difference as shown in Figure 16.

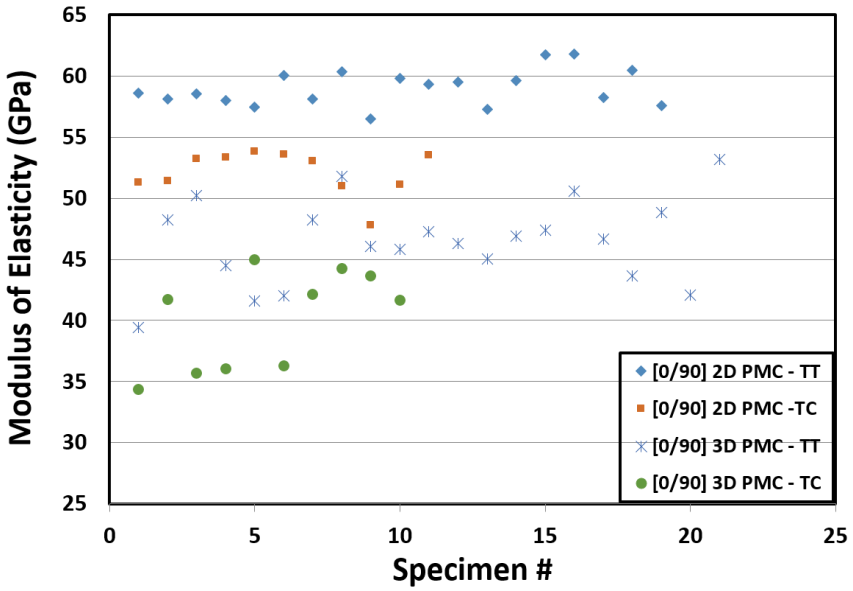

Figure 16: Room temperature modulus values for the tension-tension and tension-compression specimens. Reproduced from Wilkinson [11]

Although it occurred for both material systems, it was less obvious for the 3D PMC where the modulus values varied the most. It was assumed that this difference was a result of machining the specimens with different shapes (dogbone and hourglass shapes) and the resulting interaction between the specimen and extensometer.

The stress data acquired in compression-to-failure and tension-compression fatigue test were normalized according to Equation 5.1 in order to facilitate comparison of data for different specimen. Those stresses were normalized as in Formula 5.1:

$$\sigma_{normalized} = \sigma_{actual} \frac{E_{avg}}{E_{specimen}} \tag{5.1}$$

where $\frac{E_{avg}}{E_{specimen}}$ is the normalization ratio for a given specimen. A specimen was considered to be stiffer (higher modulus) when the normalization ratio was less than one. For consistency and a fair comparison normalized stress and normalized elastic moduli was used analyzing the data.

5.2 Thermal Expansion

All elevated temperature tests were conducted with a temperature of 329°C on the right side of the specimen, T_{right}, where the temperature was ramped to a set point at a rate of 10°C/min and then held constant for 45 min at zero load. Strain data was collected during the temperature ramp up and dwell periods. A representative example plot of the thermal stain vs. time is shown in Figure 17.

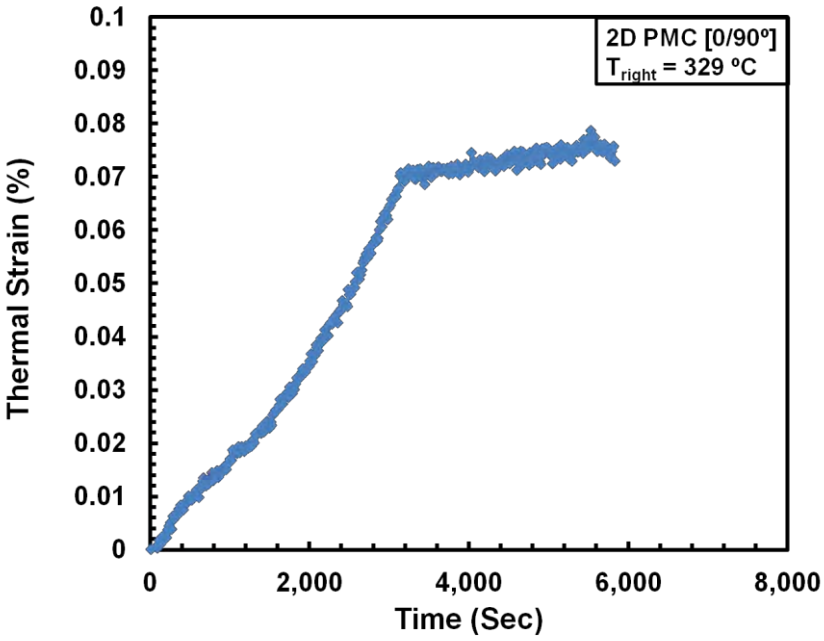

Figure 17: Thermal strain plot vs time for specimen C1-9

Thermal strains values obtained in this work are listed in Tables 12 – 13. The variation in T_{left} values can be attributed to multiple reasons, such as laboratory ambient temperature, specimen thickness, furnace position relative to the specimen, etc..

Table 12: Thermal strain data for 3D PMC with 0/90° fiber orientation

Fiber Orientation	Specimen #	T_{left} (°C)	T_{right} (°C)	Thermal Strain (%)
[0/90]	C3-3	188	329	0.068
	C3-4	195	329	0.099
	C3-5	195	329	0.056
	C3-6	199	329	0.030
	C3-7	185	329	0.009
	C3-8	188	329	0.032
	C3-9	190	329	0.042
	C3-10	190	329	0.042
	Average:	**191**	**329**	**0.047**

Table 13: Thermal strain data for 2D PMC with 0/90° fiber orientation

Fiber Orientation	Specimen #	T_{left} (°C)	T_{right} (°C)	Thermal Strain (%)
[0/90]	C1-4	215	329	0.060
	C1-5	195	329	0.057
	C1-6	200	329	0.023
	C1-7	196	329	0.139
	C1-8	200	329	0.047
	C1-10	190	329	0.073
	C1-11	200	329	0.076
	Average:	**199**	**329**	**0.068**

5.3 Monotonic Compression Tests

In order to form a baseline for the compression properties of the material systems investigated in this research effort, compression to failure tests were conducted at room temperature and at elevated temperature, T_{right}, of 329°C. Compression-to-failure test results for the two material systems are summarized in Tables 14 and 15, where elastic modulus, compressive strength, and failure strain are presented. Note that compressive modulus of elasticity was determined as the slope of best fit line of the initial linear region of a stress-strain curve. A dramatic instantaneous drop in stress was evidence of specimen failure.

Table 14: Summary of compressive properties for 3D PMC 0/90° at room temperature and elevated temperature (T_{right} = 329°C)

Fiber oriantation	Specimen #	Temperature (°C)	Elastic Modulus (GPa)	Normalized Modulus (GPa)	UCS (MPa)	Normalized UCS (MPa)	Failure Strain (%)
[0/90]	C3-2	24 / 24	41.33	39.69	-262.17	-251.74	-0.759
	Room Temp Average:		**41.33**	**39.69**	**-262.17**	**-251.74**	**-0.759**
	C3-3	188 / 329	34.10	38.32	-233.57	-262.48	-0.774
	C3-4	195 / 329	34.00	37.83	-214.91	-239.12	-0.745
	Elev Temp Average:		**34.05**	**38.08**	**-224.24**	**-250.80**	**-0.759**

Table 15: Summary of compressive properties for 2D PMC 0/90° at room temperature and elevated temperature (T_{right} = 329°C)

Fiber oriantation	Specimen #	Temperature (°C)	Elastic Modulus (GPa)	Normalized Modulus (GPa)	UCS (MPa)	Normalized UCS (MPa)	Failure Strain (%)
[0/90]	C1-3	25 / 25	50.48	49.43	-419.2	-410.5	-1.005
	Room Temp Average:		**50.48**	**49.43**	**-419.2**	**-410.5**	**-1.005**
	C1-4	215 / 329	46.10	45.02	-276.7	-270.3	-0.948
	C1-5	195 / 329	42.72	41.37	-268.3	-259.8	-0.982
	Elev Temp Average:		**44.41**	**43.19**	**-272.5**	**-265.0**	**-0.965**

5.3.1 Monotonic Compression at Room Temperature

Due to a limited number of test specimens, only one compression-to-failure test at room temperature was performed for each material system. The specimens were loaded axially along the 0° direction (warp yarns direction). The stress-strain curve obtained for specimen C3-2 (0/90° 3D PMC) is shown in Figure 18.

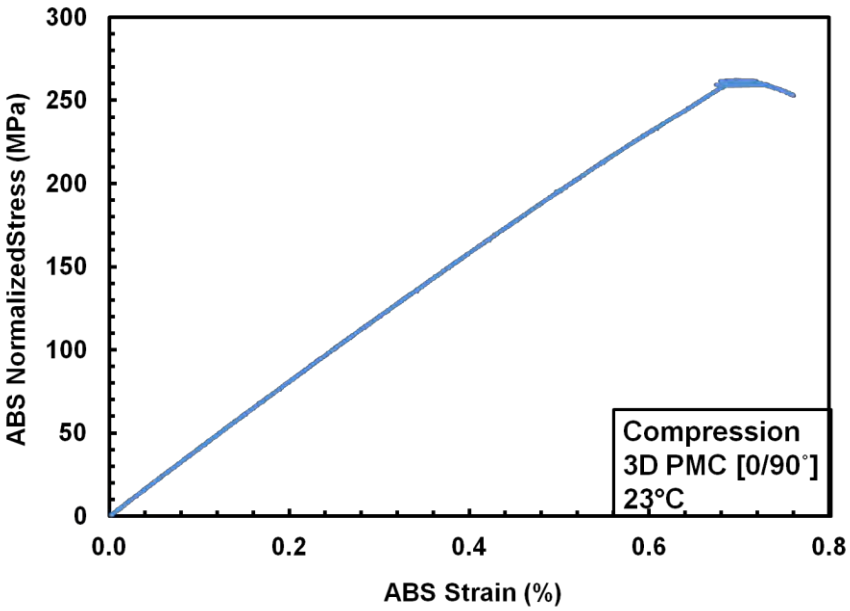

Figure 18: Compressive stress-strain curve obtained for 3D PMC 0/90° fiber orientation (specimen C3-2).

The stress-strain response obtained in monotonic compression for the 3D PMC with 0/90° fiber orientation is compared with the stress-strain results obtained in monotonic tension by Wilkinson [11] in Fig. 19. The specimen tested in compression showed a nearly linear response for most of the stress-strain history. Contrastingly, the tensile stress-strain curves obtained by Wilkinson [11] show a non-linear increase in modulus. Notably, the compressive strength is nearly 68% less than the UTS. Likewise, the failure strain in compression is approximately half of the failure strain produced in tension. Finally, the tensile modulus is approximately 7.6 GPa higher than the compressive modulus.

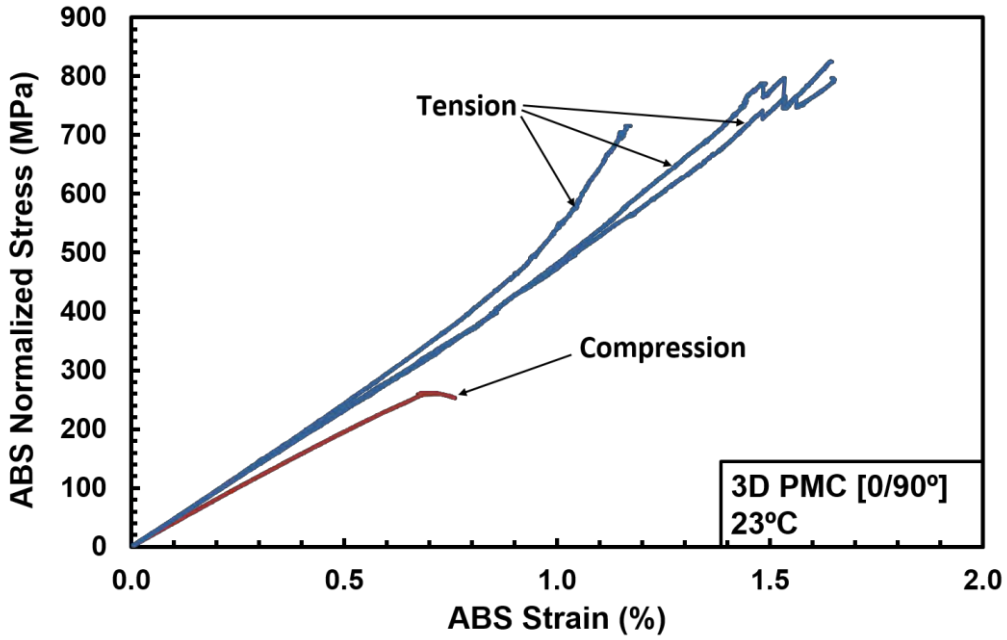

Figure 19: Tensile and compressive stress-strain curves obtained for the 3D PMC with 0/90° fiber orientation at room temperature. Tension results from Wilkinson [11].

Due to a limited number of test specimens, only one 2D PMC specimen with 0/90° fiber orientation was tested in compression to failure at room temperature. The compressive stress-strain response of the 2D PMC with 0/90° fiber orientation is shown in Figure 20. The normalized UCS was -410.5 MPa and compressive modulus was 49.43 GPa. Notably, the UCS of the 2D PMC with 0/90° fiber orientation was nearly 39% higher than the UCS of the 3D PMC with 0/90° fiber orientation. Likewise, the compressive modulus of the 2D PMC was approximately 9.74 GPa greater than that of the 3D PMC. A comparison of compression stress-strain curves obtained for the 2D and 3D PMCs with 0/90° fiber orientation is depicted in Figure 21. Compressive stress-strain behavior of the 2D PMC with 0/90° fiber orientation was similar to that of the 3D PMC

with 0/90° fiber orientation. In both 2D and 3D composites, the matrix is likely to play a major role in sustaining the compressive load with little contribution from the fibers.

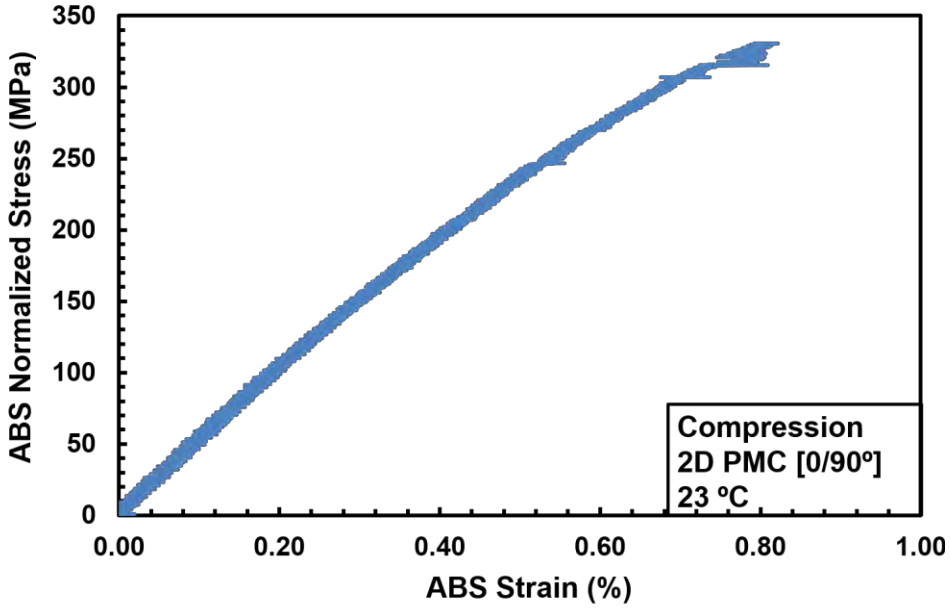

Figure 20: Compressive stress-strain curve obtained for 2D PMC 0/90° fiber orientation at room temperature

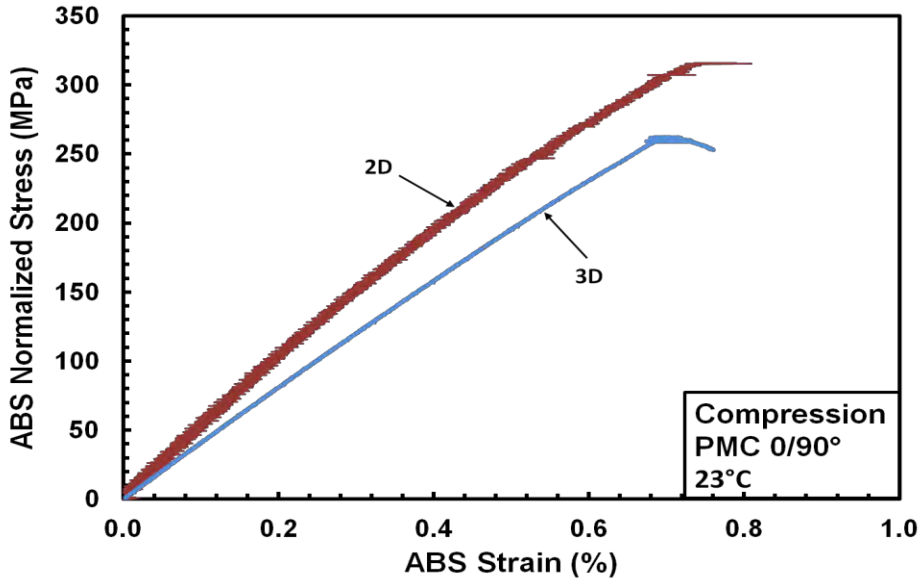

Figure 21: Compressive stress-strain curves for 2D and 3D PMCs with 0/90° fiber orientation at room temperature

The tensile and compressive stress-strain curves obtained for the 2D PMC with 0/90° fiber orientation at room temperature are shown in Figure 22. Compressive modulus of the 2D PMC is about 13.7% lower than its tensile modulus. Furthermore, the normalized UCS of the 2D PMC is only about 49% of its normalized UTS.

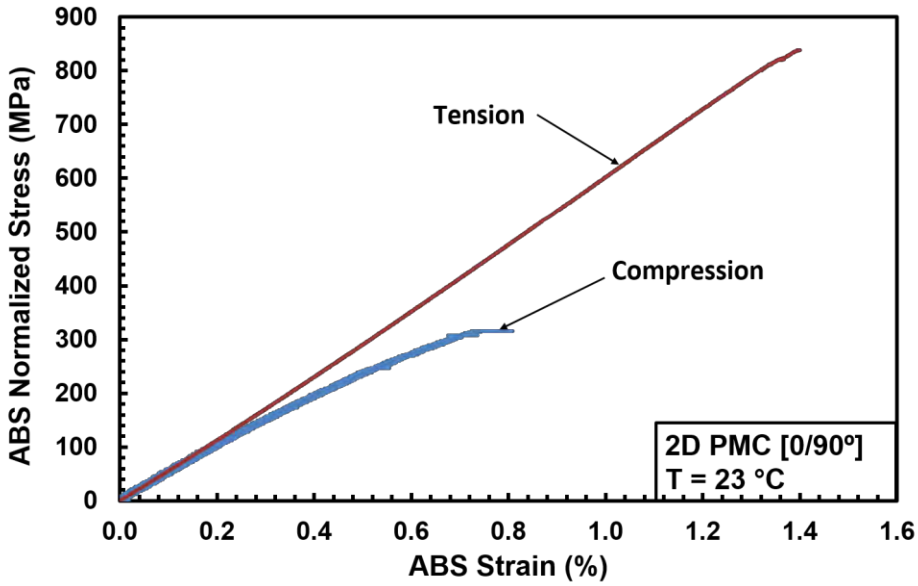

Figure 22: Tensile and compressive stress-strain curves for 2D PMC with 0/90° fiber orientation at room temperature. Tension results from Wilkinson [11].

The tensile and compressive stress-strain curves obtained for the 2D and 3D PMCs with 0/90° fiber orientation at room temperature are shown in Figure 23.

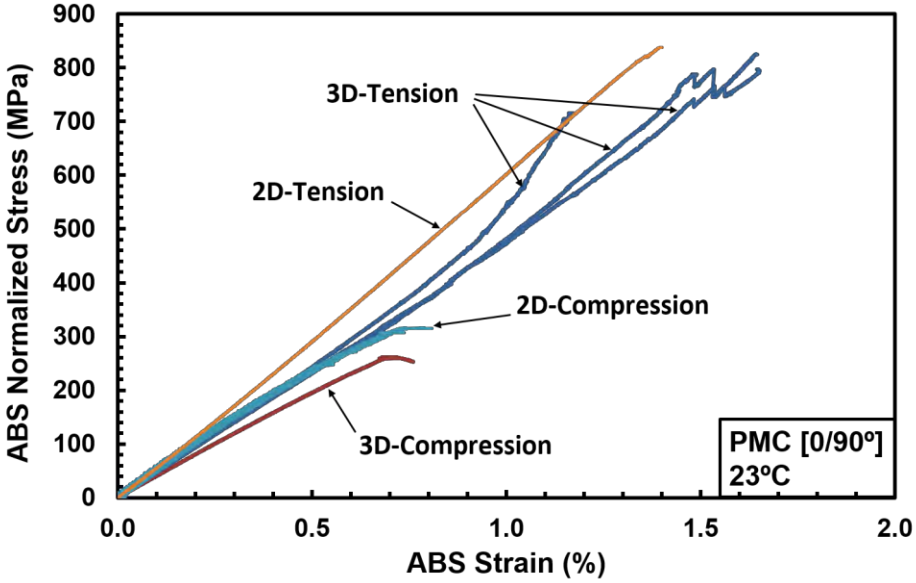

Figure 23: Tensile and Compressive stress-strain obtained for 2D and 3D PMCs with 0/90° fiber orientation at room temperature. Tension results from Wilkinson [11].

In summary, the room temperature compression-to-failure results showed that the 2D PMC with 0/90° fiber orientation had higher compressive strength (UCS) and compressive stiffness (modulus) than the 3D PMC with 0/90° fiber orientation, as was the case in tension-to-failure tests. While the 3D PMC with 0/90˚ showed a nearly linear response, the compressive stress-strain curves obtained for the 2D PMCs with 0/90° fiber orientation showed a progressive drop in the stiffness. In contrast the tensile stress-strain curves of the 3D PMC with 0/90° fiber orientation showed an increase in the modulus, whereas the 2D PMC with 0/90° exhibited a linear stress-strain behavior till failure.

5.3.2 Monotonic Compression at Elevated Temperature

Two compression-to-failure tests were conducted for each material system at an elevated temperature of 329°C. Note that unheated side of the specimen fluctuated from test to test since it was open to the ambient air. The results obtained in compression-to-failure tests are summarized in Tables 14 and 15 in section 5.3. As seen in Figure 24, the stress-strain curves obtained in monotonic compression for the 3D PMC at elevated temperature are similar to those obtained at room temperature. It was determined that the compressive properties of the 3D PMC are little affected by temperature. It is noteworthy, that Wilkinson [11] reported that the tensile properties and the tensile stress-strain response of the 3D PMC also appeared to be independent of temperature.

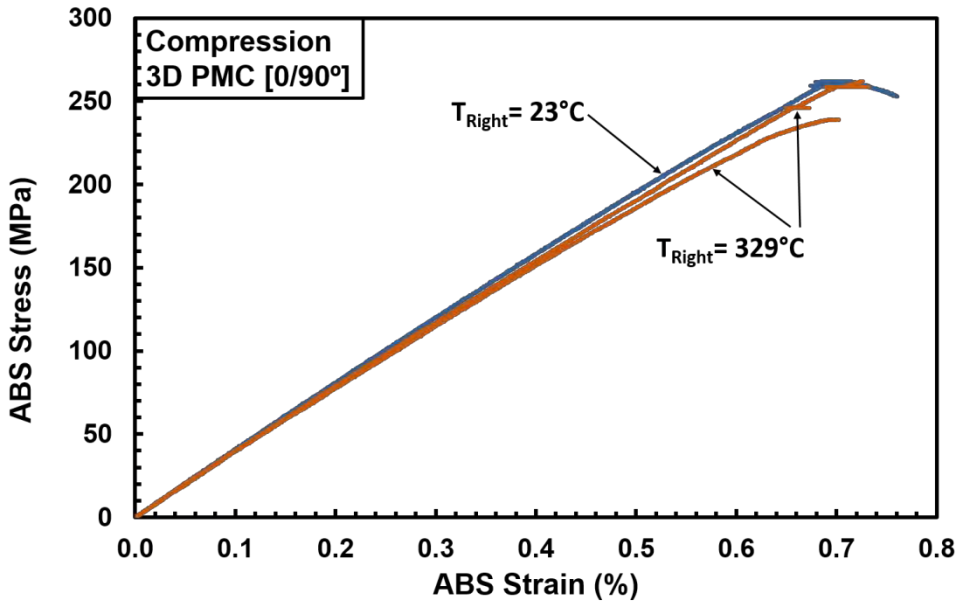

Figure 24: Compressive stress-strain response obtained for 3D PMC with 0/90° fiber orientation at room and elevated temperature

Compressive stress-strain curves obtained for the 2D PMC at elevated temperature are compared to those obtained at room temperature in Figure 25. Stress-strain curves obtained in monotonic compression for both material systems at room and elevated temperature are combined in Figure 26. It is seen in Figure 26 that the room-temperature compressive strength and modulus are higher than the respective elevated-temperature values. Yet, the difference is not dramatic. As in the case of the 3D PMC, compression properties and stress-strain behavior of the 2D PMC are only slightly affected by temperature. Similar conclusions were reached by Wilkinson [11] regarding tensile properties and tensile stress-strain behavior of the two material systems. Figure 27 compares the tensile and compressive stress-strain curves obtained for the 3D PMC at room and elevated temperature, where Figure 28 compares those of the 2D PMC.

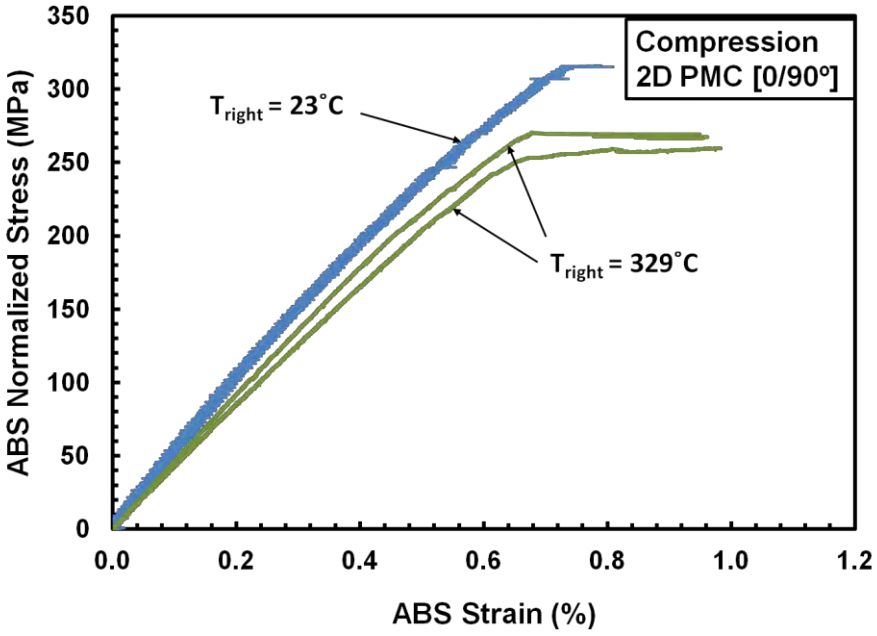

Figure 25: Compressive stress-strain response obtained for 2D PMC with 0/90° fiber orientation at room and elevated temperature

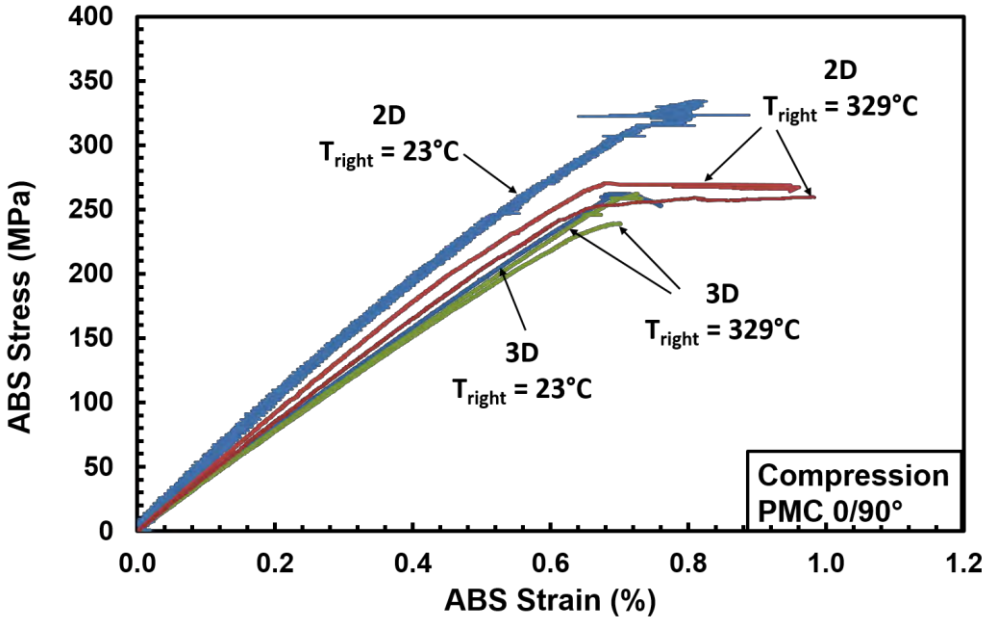

Figure 26: Compressive stress-strain response obtained for 3D and 2D PMCs with 0/90° fiber orientation at room and elevated temperature

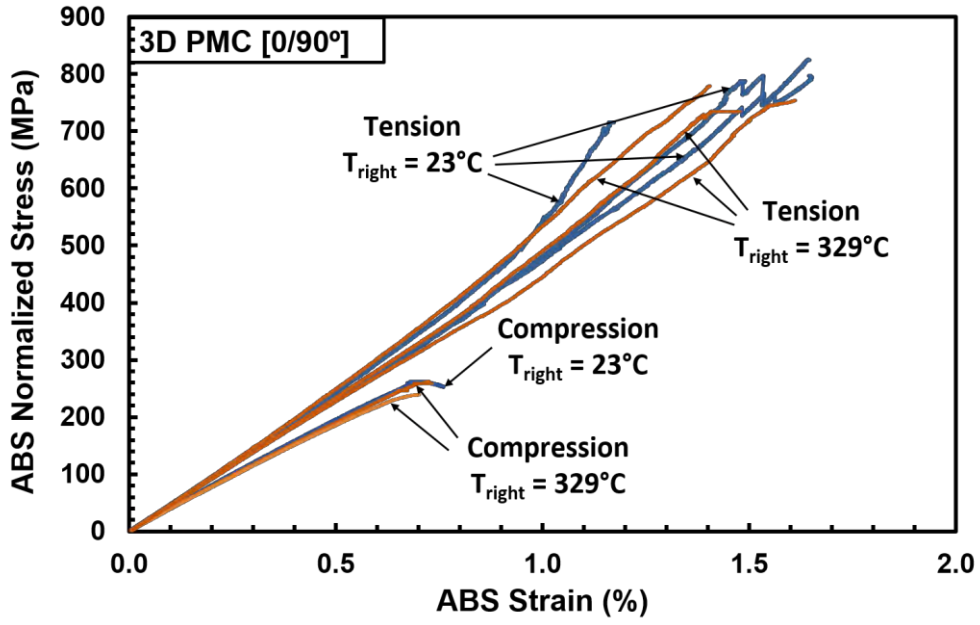

Figure 27: Tensile and compressive stress-strain responses obtained for 3D PMC with 0/90° fiber orientation at room and elevated temperature. Tension results from Wilkinson [11].

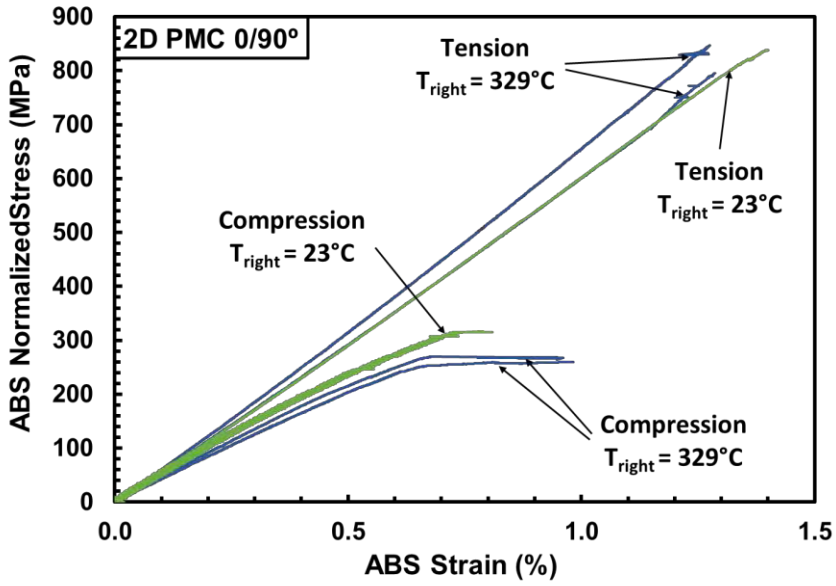

Figure 28: Tensile and compressive stress-strain responses obtained for 2D PMC with 0/90° fiber orientation at room and elevated temperature. Tension results from Wilkinson [11].

Figure 29 compares compressive stress-strain responses of the 3D and 2D PMCs with 0/90° fiber orientation. The normalized UCS of the 2D PMC is somewhat greater than the normalized UCS of the 3D PMC. Additionally, the compressive modulus of the 2D PMC is 11.8% higher than that of the 3D PMC. Finally, the failure strain of the 2D PMC exceeds that of the 3D PMC by some 21.3%.

Figure 30 compares tensile stress-strain behavior of the 3D PMC and of the 2D PMC with 0/90° fiber orientation at elevated temperature. The average UTS of the 2D PMC is 8.6% greater than the average UTS of the 3D PMC. The 2D PMC is also stiffer, with the average modulus being 27% greater than that of the 3D PMC. These differences in UTS and modulus are similar to the differences observed at room temperature. The 3D PMC also exhibited greater failure strains than the 2D PMC (approximately 14.8% greater).

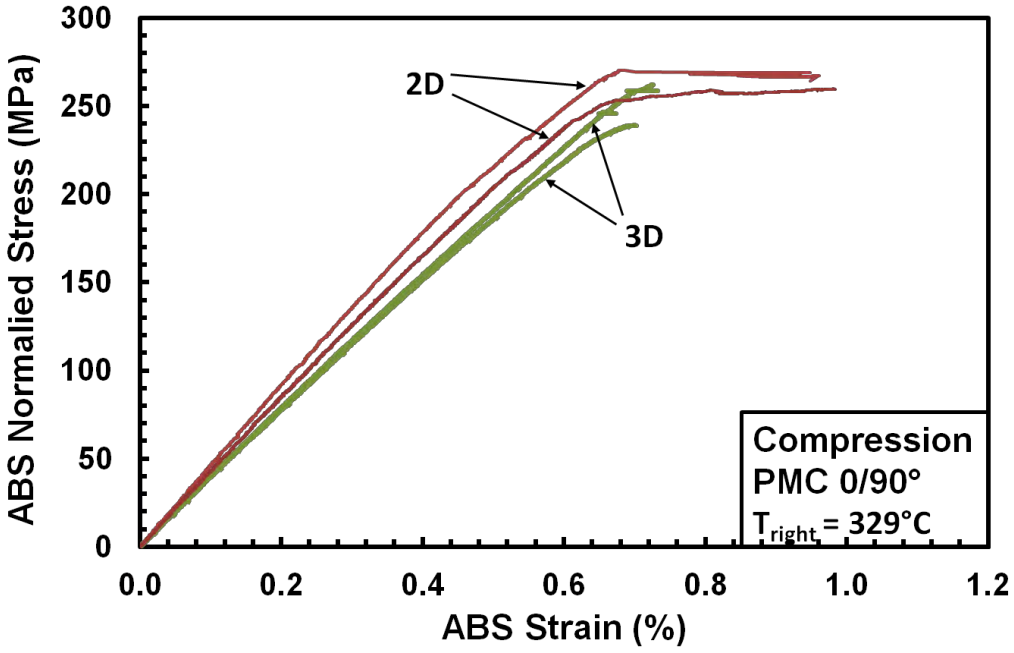

Figure 29: Compressive stress-strain response obtained for 2D and 3D PMC with 0/90 fiber orientation at elevated temperature

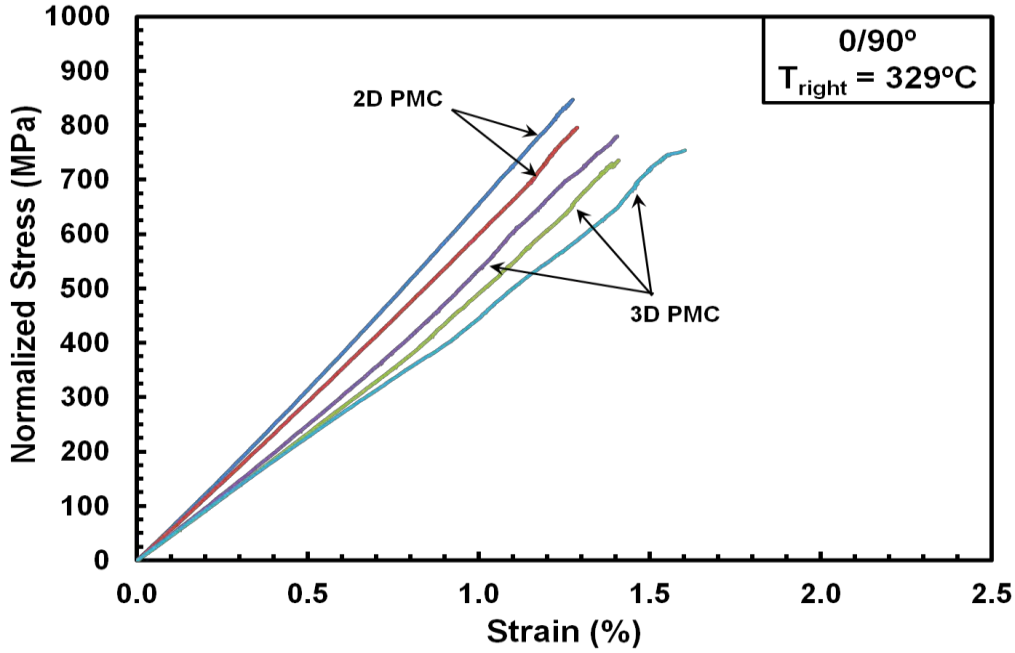

Figure 30: Tensile stress-strain response obtained for 2D and 3D PMC with 0/90 fiber orientation at elevated temperature. Results reproduced from Wilkinson [11]

The compressive stress-strain results obtained for these material systems at elevated temperature are compared with the elevated-temperature tensile stress-strain results obtained by Wilkinson [11] in Figures 31. The 2D PMC exhibits higher compressive strength and stiffness than the 3D PMC. Yet, for both materials, compressive strength and stiffness are below the corresponding tensile values.

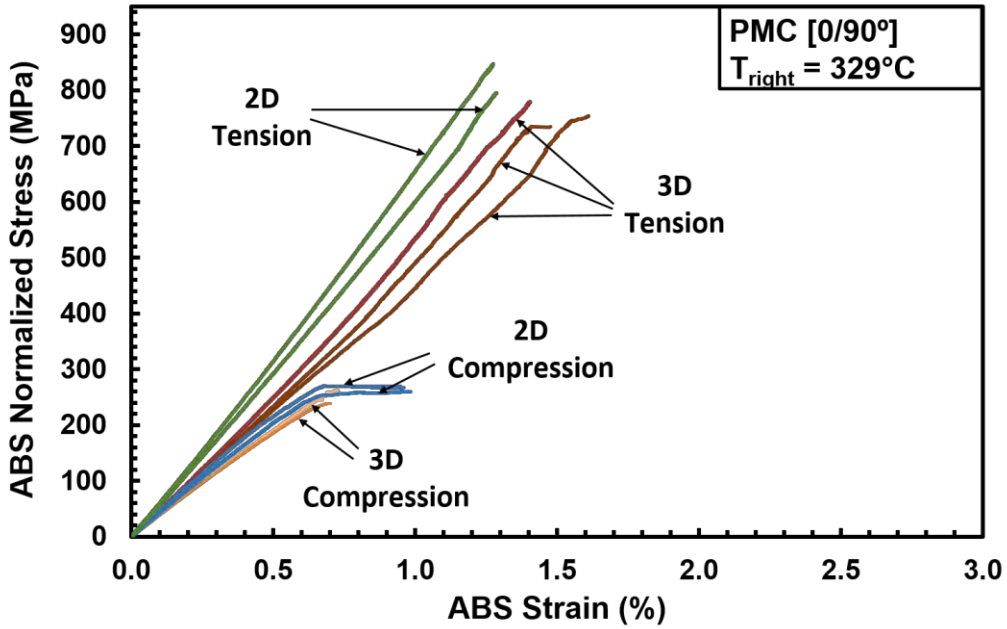

Figure 31: Tensile and compressive stress-strain responses obtained for 3D and 2D PMC with 0/90° fiber orientation at elevated temperature. Tension results from Wilkinson [11].

5.4 Tension-Compression Fatigue Results at Elevated Temperature

In this research the tension-compression fatigue behavior was investigated at elevated temperature. All tension-compression fatigue tests were carried at an elevated temperature of 329°C with a minimum to maximum stress ratio of R = -1 at the frequency of 1 Hz. Fatigue run-out was set to $2x10^5$ cycles.

5.4.1 Tension-Compression Fatigue Performance of 3D PMC with 0/90° Fiber Orientation

Table 16 summarizes tension-compression fatigue results obtained for the 3D PMC with 0/90° fiber orientation. The tension-compression fatigue run-out was achieved for the maximum stress of 198.9 MPa (79 %UCS).

Table 16: Tension-compression fatigue results for 3D PMC with 0/90° fiber orientation at 329°C

Specimen #	Maximum Stress (MPa)	Maximum Stress (% UCS)	Normalized Max. Stress (MPa)	Normalized Max. Stress (% UCS)	Cycles to Failure (N)	Failure Strain (%)	Modulus Loss (%)
C3-1	210.2	94	245.1	98	14,915	-0.720	9.394
C3-10	220.2	98	211.8	84	12,608	-1.485	-43.519
C3-8	220.2	98	199.5	80	1,333	-0.630	-11.141
C3-6	180.2	80	198.9	79	200,000	-0.649^{NF}	-33.633
C3-9	210.1	94	193.0	77	16,662	-0.351	-0.951
C3-7	202.6	90	192.6	77	200,000	-0.508^{NF}	-1.815
C3-5	160.4	72	142.9	57	200,000	-0.272^{NF}	3.821

^{NF}: No Failure during fatigue. Specimen achieved run-out defined as $2x10^5$ cycles.

Tension-compression fatigue results for the 3D PMC are shown as the maximum stress vs. cycles to failure (S-N) curve in Figure 32a. Included in Figure 32a are the tension-tension fatigue results reported by Wilkinson [11]. Not surprisingly, the 3D PMC

with 0/90° fiber orientation exhibits better fatigue performance under tension-tension cycling, where the high-stiffness, high-strength fibers control the composite response. Conversely, a comparatively weak polymer matrix controls the composite response during the compression portion of the cycle in tension-compression fatigue. It is instructive to assess the fatigue performance of the composite relative to the composite strength, i. e. the UTS for tension-tension cycling and the UCS in the case of tension-compression cycling. This is accomplished by plotting maximum stress as %UTS (%UCS for tension-compression fatigue) on the S-N plot (see Figure 32b). Results in Figure 33b reveal that the S-N curves obtained in tension-compression and in tension-tension fatigue occur at similar percentages of the corresponding ultimate strength value. Still the tension-compression fatigue run-out limit was achieved at a somewhat higher percentage of the corresponding strength value (79%UCS) than the tension-tension fatigue run-out limit (64%UTS).

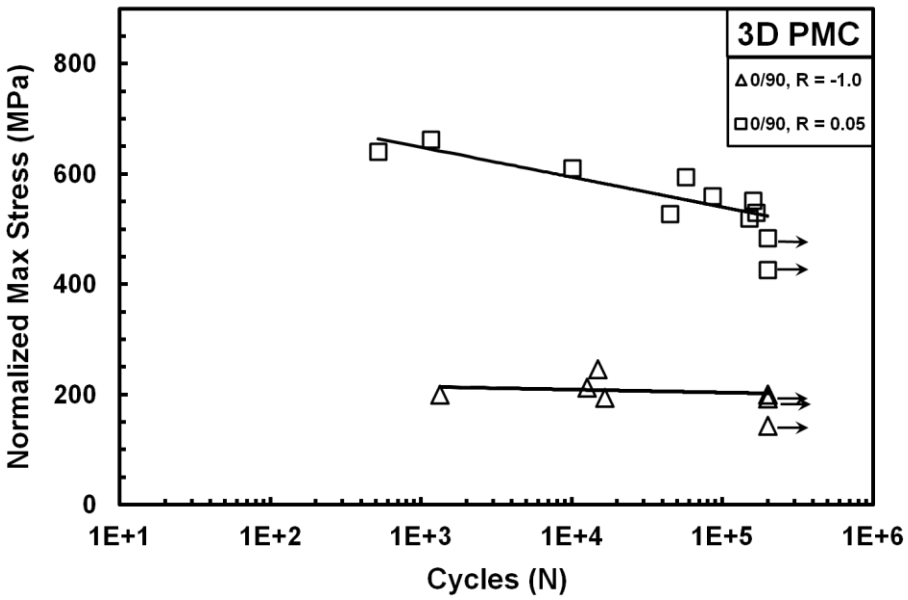

(a)

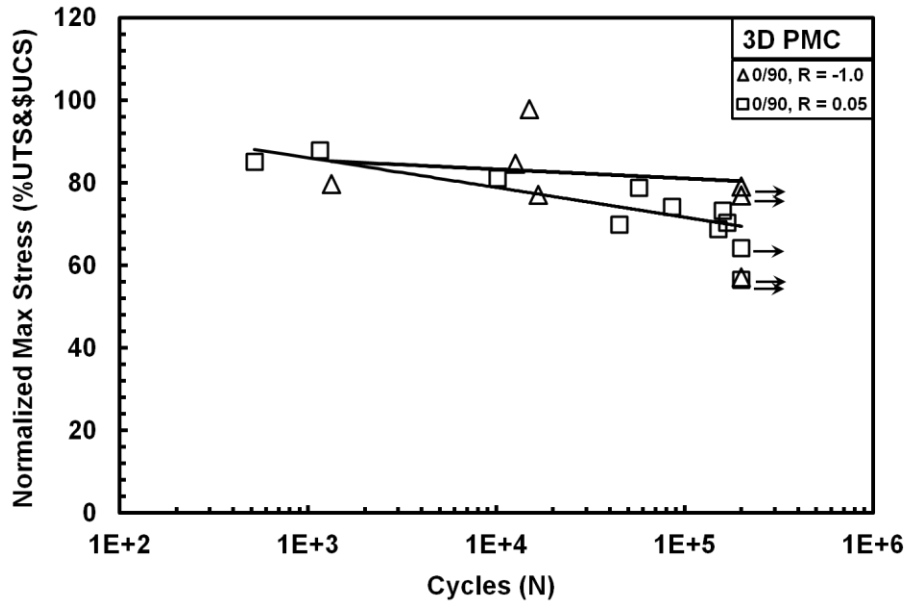

(b)

Figure 32: S-N curves obtained for the 0/90˚ 3D PMC with at elevated temperature. (a) Stress is shown in units of MPa, (b) stress is shown in units of %UTS or %UCS. Arrow indicates that fatigue run-out was achived. Tension-tension fatigue results from Wilkinson [11].

The tension-compression fatigue results obtained for the 3D PMC with 0/90˚ fiber orientation in this research are also compared to the tension-tension fatigue results reported by Wilkinson [11] for the 3D PMC with ±45° fiber orientation (see Figure 33). The matrix plays a significant role during both tension-compression fatigue of the 0/90 composite and the tension-tension fatigue of the ±45 composite.

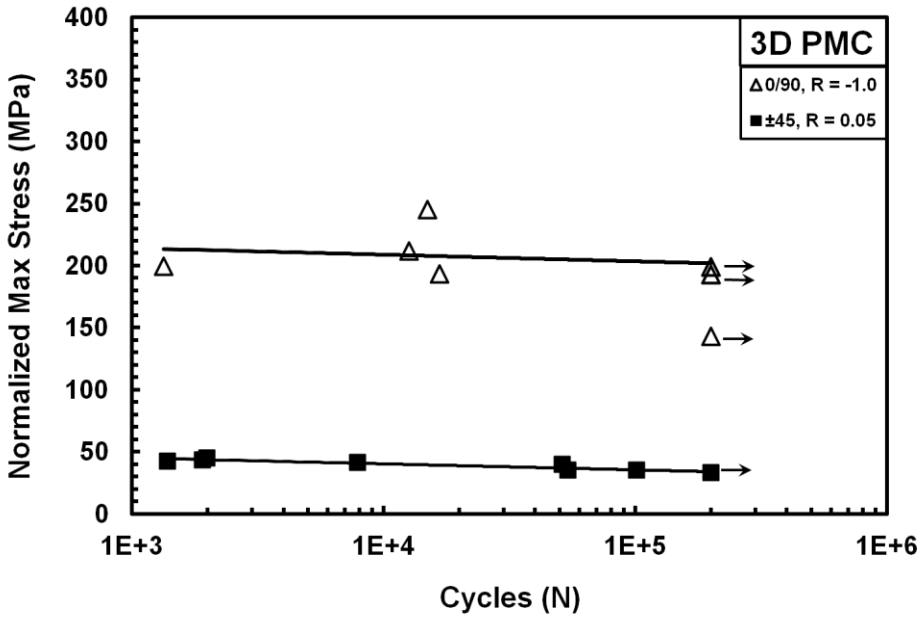

Figure 33: A comparison of the S-N curves obtained in tension-compression fatigue for the 0/90 3D PMC and in tension-tension fatigue for the ±45 3D PMC. All tests were performed at elevated temperature. Arrow indicates that fatigue run-out was was achieved. Tension-tension fatigue results from Wilkinson [11].

Results in Figure 33 reveal that the tension-compression fatigue performance of the 0/90 3D PMC exceeds the tension-tension fatigue performance of the ±45 3D PMC. This result is hardly surprising. Recall that the relatively weak matrix dominates the entire cycle of the tension-tension fatigue test of the composite with ±45° fiber orientation. In contrast, the matrix only governs 1/2 the tension-compression fatigue test of the composite with 0/90 fiber orientation. While the matrix dominates the 0/90

composite response during the compression portion of the cycle, fibers dominate the 0/90 composite response during the tension portion of the cycle.

Evolution of the hysteresis stress-strain response of the 3D PMC with 0/90° fiber orientation during tension-compression fatigue is presented in Figures 34 and 35 for the normalized maximum stresses of 192.6 MPa and 211.8 MPa, respectively. Notably, the hysteresis stress-strain loops shown in Figure 34 typify the hysteresis stress-strain response produced in all tests that achieved fatigue run-out of $2x10^5$ cycles. Results in Figure 34 show little strain accumulation and little modulus loss with cycling. The results in Figure 35 show that while little strain accumulation occurred in the 212 MPa test, considerable modulus loss is observed. It is noteworthy that the stress-strain response in Figure 35 remains symmetric with respect to the origin. Additional plots of the hysteresis stress-strain response produced in tension-compression fatigue tests are given in the Appendix A.

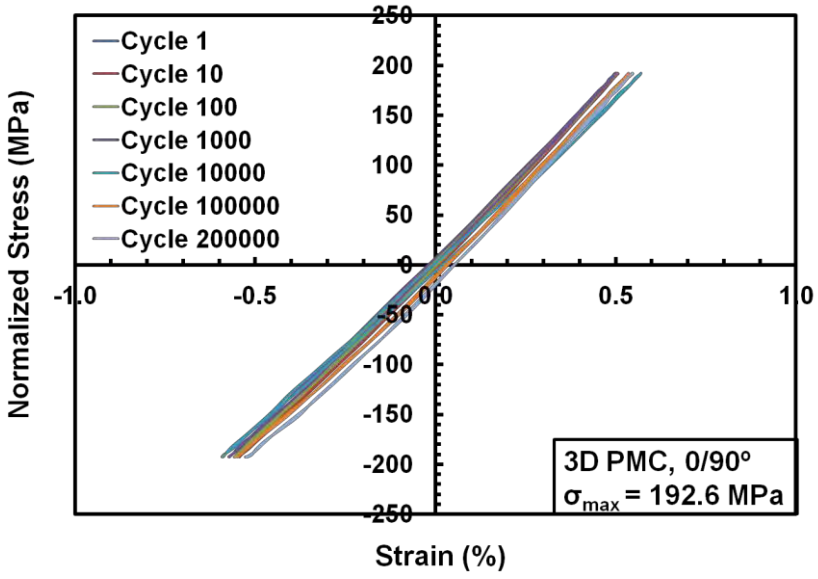

Figure 34: Evolution of stress-strain hysteresis response with fatigue cycles for specimen C3-7 of the 3D PMC with 0/90° fiber orientation at elevated temperature.

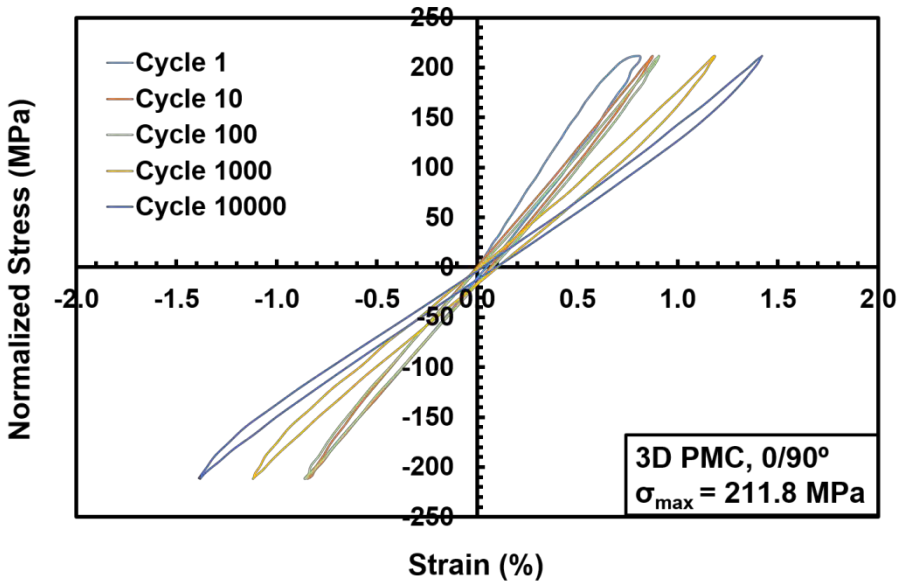

Figure 35: Evolution of stress-strain hysteresis with fatigue cycles for specimen C3-10 of the 3D PMC with 0/90° fiber orientation at elevated temperature.

Of importance in cyclic fatigue is the reduction in stiffness (hysteresis modulus determined from the maximum and minimum stress-strain data points during a load cycle), reflecting the damage development during fatigue cycling. The change in normalized modulus (i.e. modulus normalized by the modulus obtained in the first cycle) versus fatigue cycles is shown in Fig. 36. It is seen that for the maximum stress levels below 199.5 MPa, the modulus remains relatively unchanged until near failure. The modulus loss varied between -9.4% (stiffening) and 45.5% (softening). A somewhat erratic modulus behavior observed for some specimens in Figure 36 is considered to be the artifact due to the movement of the extensometer rods during fatigue loading.

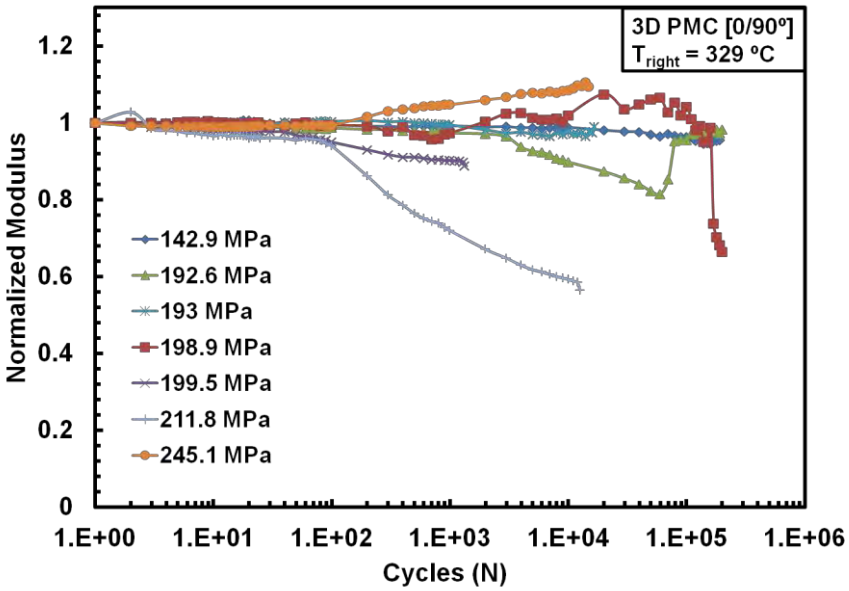

Figure 36: Normalized modulus vs. tension-compression fatigue cycles for the 3D PMC with 0/90° fiber orientation at elevated temperature.

The evolution of maximum and minimum strains with tension-compression fatigue cycles is presented in Figure 37 for the 3D PMC with 0/90° fiber orientation. In most tests, the strains remain fairly constant until near failure. Specimen C3-10 tested with the maximum normalized stress of 212 MPa (84% of normalized UCS) represents an exception. In the 212 MPa test, considerable increases in tensile and compressive strains were observed.

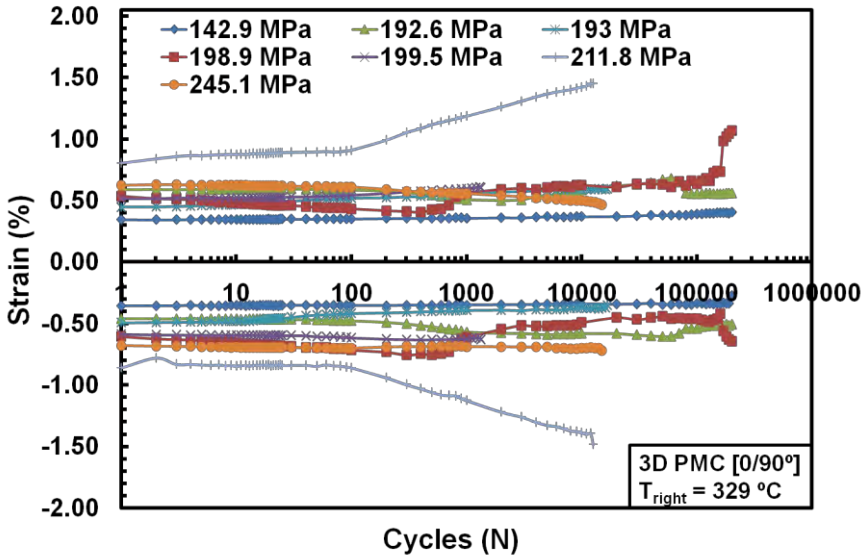

Figure 37: Maximum and minimum strain vs. tension-compression fatigue cycles for the 3D PMC with 0/90° fiber orientation at elevated temperature.

5.4.2 Tension-Compression Fatigue performance of 2D PMC with 0/90° fiber orientation

Table 17 summarizes tension-compression fatigue results obtained for the 2D PMC with 0/90° fiber orientation. The tension-compression fatigue run-out was achieved for the maximum normalized stress of 161.5 MPa (61% of normalized UCS).

Table 17: Tension-compression fatigue results for 2D PMC with 0/90° fiber orientation at T_{right} = 329˚C.

Specimen #	Maximum Stress (MPa)	Maximum Stress (% UCS)	Normalized Max. Stress (MPa)	Normalized Max. Stress (% Normalized UCS)	Cycles to Failure (N)	Failure Strain (%)	Modulus Loss (%)
C1-9	240.9	88	262.8	99	12,130	-0.400	11.621
C1-11	250.1	92	243.6	92	17,155	-1.167	22.515
C1-8	233.0	86	238.0	90	10,279	-0.810	27.993
C1-6	216.3	79	210.5	79	13,757	-0.546	14.279
C1-10	190.6	70	194.2	73	42,944	-0.552	28.451
C1-7	164.5	60	161.5	61	200,000	-0.256	7.295

Figure 38a shows the tension-compression fatigue results obtained for the 2D PMC with 0/90° fiber orientation are shown as the maximum stress vs. cycles to failure (S-N) curve. Included in Figure 38a are the tension-tension fatigue results reported by Wilkinson [11]. Results in Figure 38b reveal that the S-N curves obtained in tension-compression fatigue occur at lower percentages of the corresponding ultimate strength value compared to that of the tension-tension fatigue for percentage value up to ~90%, and then the S-N curve obtained in tension-compression fatigue exhibited better performance. Figure 39 compares the S-N curves obtained for the 2D PMC with 0/90° fiber orientation in tension-compression fatigue with the S-N curves obtained for the 2D PMC with 0/90 and with ±45 fiber orientations in tension-tension fatigue by Wilkinson [11]. As in the case of the 3D PMC, the tension-compression fatigue performance of the 0/90 2D PMC is below the tension-tension fatigue performance of the 0/90 2D PMC, but better than the tension-tension fatigue performance of the ±45 2D PMC. The fatigue limits of the 2D PMC with 0/90 in tension-compression fatigue was 161.5 MPa (61%UCS), where it was 585.3 MPa (71%UTS) and 69.4 MPa (55%UTS) for the 2D PMCs with 0/90 and with ±45 fiber orientations respectively, in tension-tension fatigue.

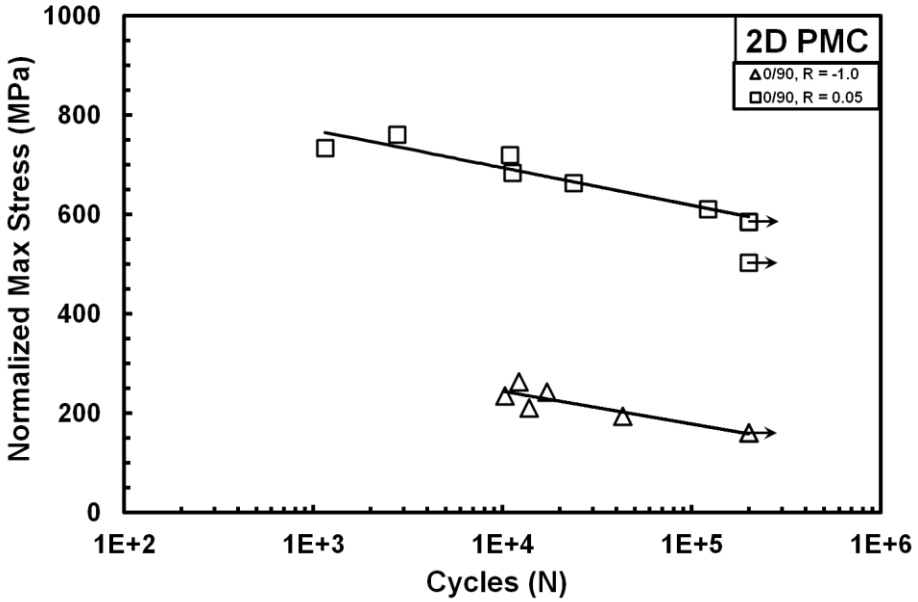

(a)

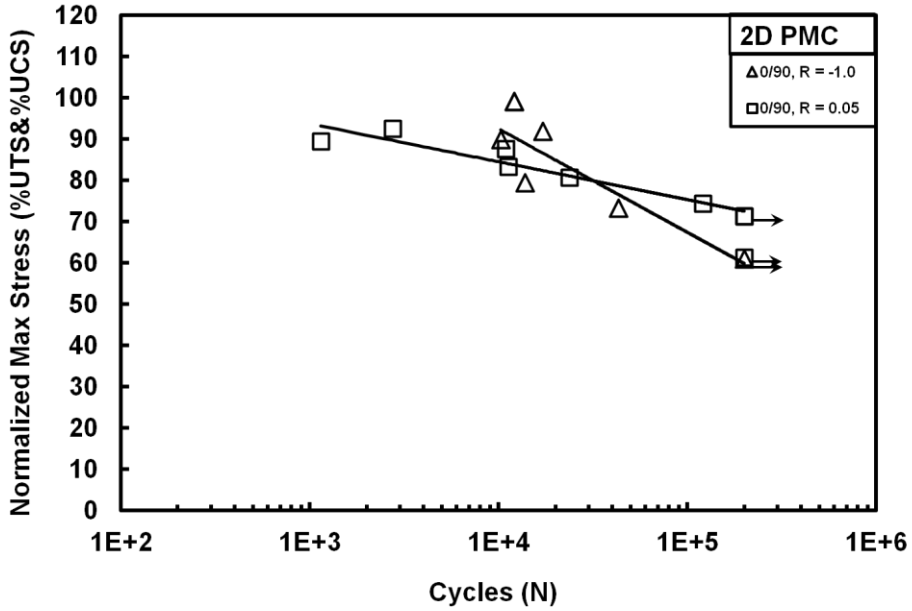

(b)

Figure 38: S-N curves obtained for the 2D PMC at elevated temperature.
(a) Stress is shown in units of MPa, (b) stress is shown in units of %UTS or %UCS.
Arrow indicates that fatigue run-out was achived. Tension-tension fatigue results from Wilkinson [11].

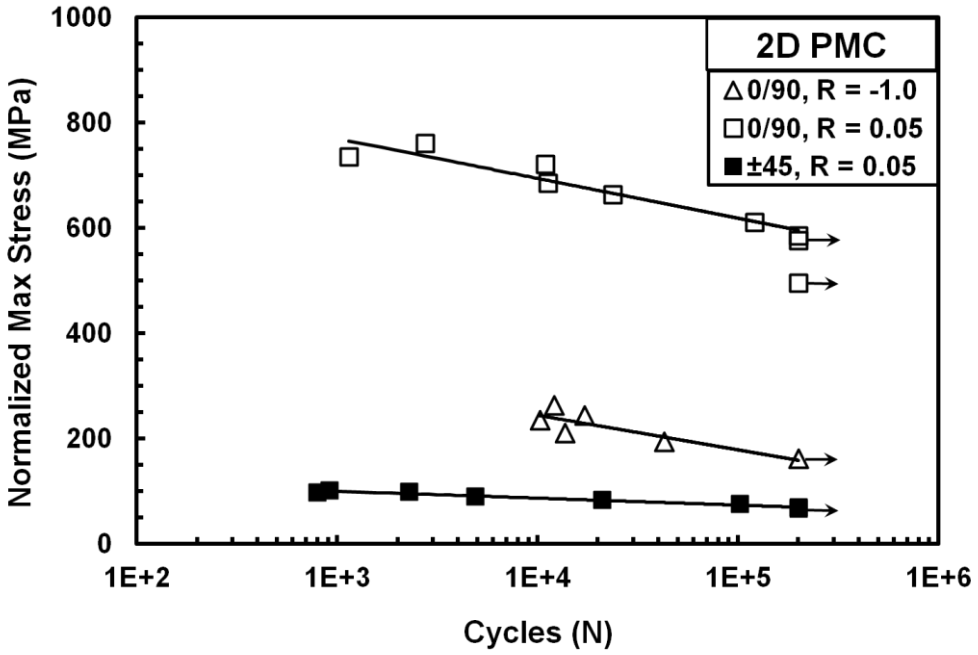

Figure 39: S-N curves for the 2D PMC at elevated temperature. Arrows indicates that fatigue run-out was achieved. Tension-tension fatigue results from Wilkinson [11].

The evolution of the hysteresis stress-strain response of the 2D PMC with 0/90° fiber orientation during tension-compression fatigue is presented in Figure 40 for the normalized maximum stresses of 162 MPa. Note that the hysteresis stress-strain loops shown in Figure 40 typify the hysteresis stress-strain response produced in all tests that achieved fatigue run-out of $2x10^5$ cycles. Results in Figure 40 show little strain accumulation and little modulus loss with cycling. Additional plots of the hysteresis stress-strain response produced in tension-compression fatigue tests are given in the Appendix A.

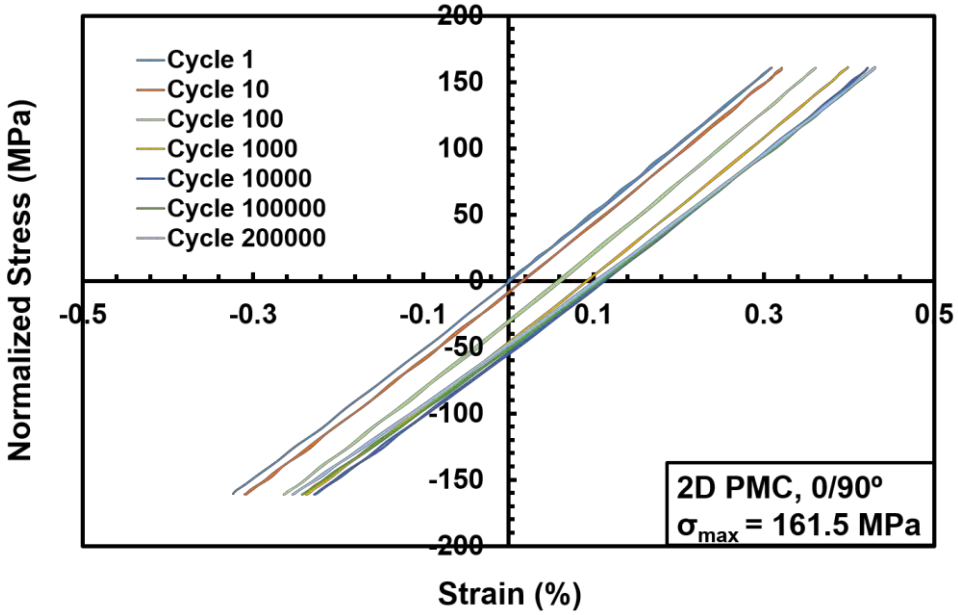

Figure 40: Evolution of stress-strain hysteresis response with tension-compression fatigue cycles obtained for specimen C1-7 of the 2D PMC with 0/90° fiber orientation at elevated temperature.

The change in normalized modulus (i.e. modulus normalized by the modulus obtained in the first cycle) with fatigue cycles for the 2D PMC with 0/90 fiber orientation is shown in Fig. 41. It is seen that for the modulus remains relatively unchanged until near failure, where a decrease in modulus is observed. The modulus loss varied between 7% and 28%. In contrast to the 3D PMC, the 2D PMC did not show any stiffening at the end of the fatigue life time.

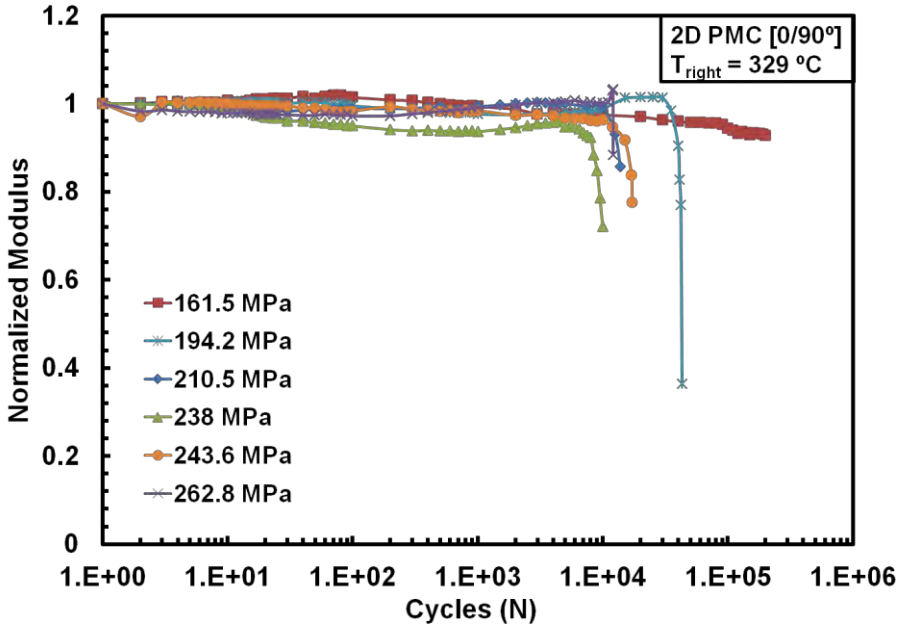

Figure 41: Normalized modulus vs. tension-compression fatigue cycles for the 2D PMC with 0/90° fiber orientation at elevated temperature.

The evolution of maximum and minimum strains with tension-compression fatigue cycles for the 2D PMC with 0/90° fiber orientation is presented in Figure 42. In most tests, the strains remain fairly constant until near failure. Specimen C1-11 tested with the maximum normalized stress of 244 MPa represents an exception. In the 244 MPa test, considerable accumulation of compressive strain was observed.

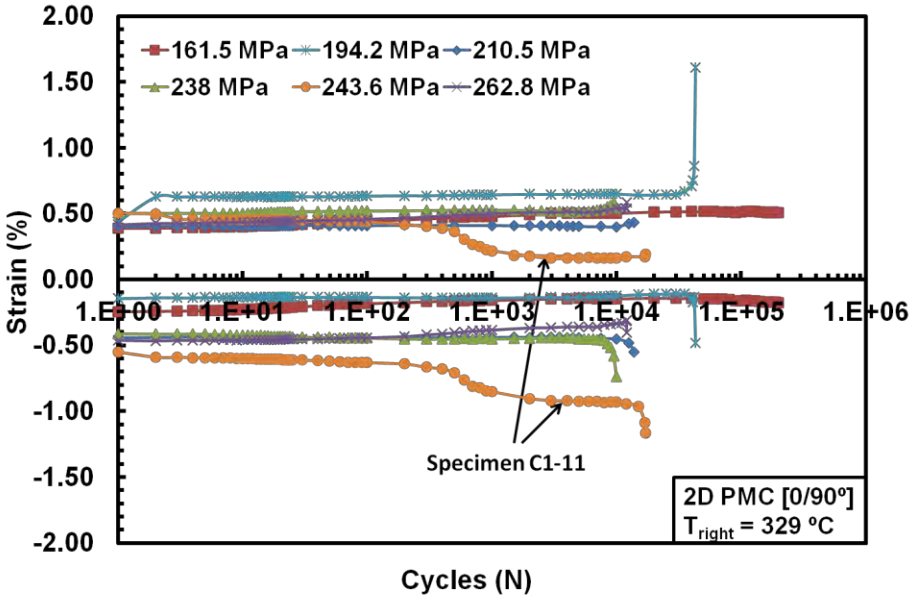

Figure 42: Maximum and minimum strain vs. tension-compression fatigue cycles for the 2D PMC with 0/90° fiber orientation at elevated temperature.

5.4.3 Comparison of Tension-Compression Fatigue Performance of the 3D and 2D PMCs with 0/90 Fiber Orientation.

The S-N curves obtained for the 3D and 2D PMCs are used to compare the fatigue performance of the two material systems in Figure 43. Although the 3D PMC exhibits lower compressive strength than the 2D composite, the fatigue limit obtained for the 3D PMC is 19% higher than the fatigue limit obtained for the 2D PMC. However, the 2D PMC exhibits better fatigue performance at higher maximum stress levels. The tension-compression S-N curves obtained for the two composites are also compared in Figure 44, where the maximum stress is shown as %UCS. The results in Figure 44 show that relative to the UCS, the 3D PMC still exhibits a higher fatigue limit, while the 2D PMC exhibits better performance at higher maximum stresses.

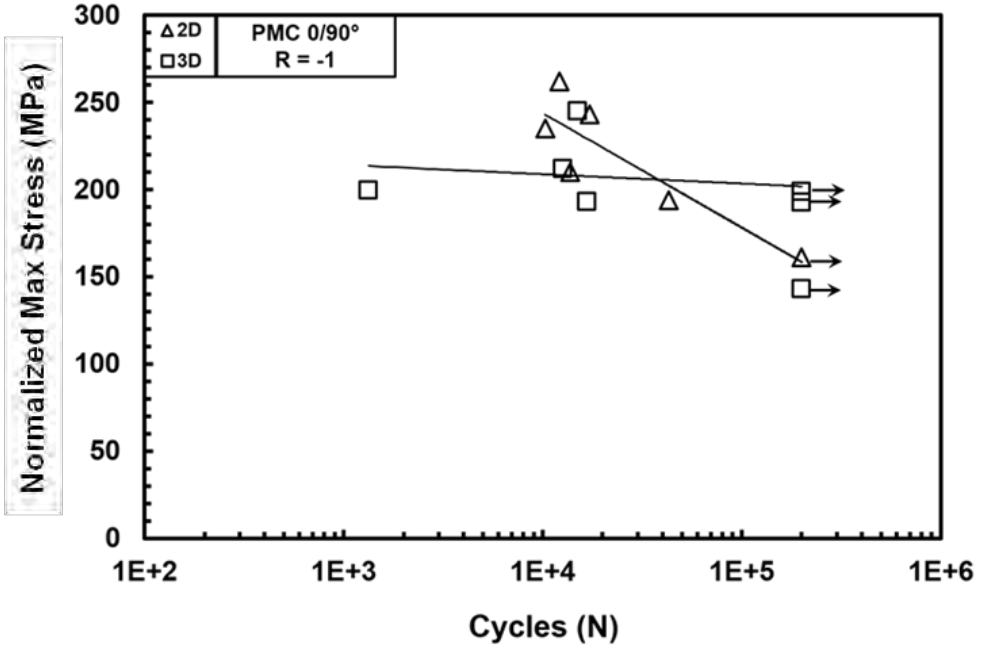

Figure 43: S-N curves obtained for the 3D and 2D PMCs with 0/90 fiber orientation in tension-compression fatigue at elevated temperature. Arrows indicates fatigue run-out was achieved.

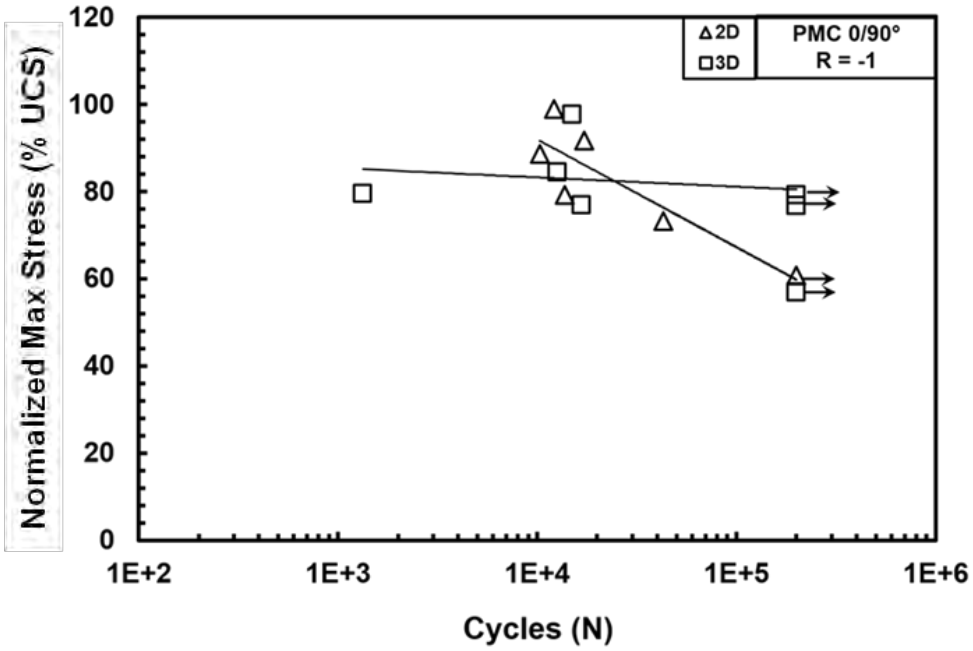

Figure 44: S-N curves obtained for the 3D and 2D PMC with 0/90 fiber orientation in tension-compression fatigue at elevated temperature. Arrows indicates fatigue run-out was achieved. Stress is shown as %UCS

5.5 Retained Tensile Properties Post-Fatigue.

All specimens that achieved fatigue run-out of 2 x 10^5 cycles were subjected to tension-to-failure test at elevated temperature of 329°C in order to assess their retained tensile properties. Only one tension-to-failure test was successful (specimen C3-6) where the specimen failed in tension and broken to two parts. The tension tests failed due to failure in the specimen grip section after surviving fatigue of 200,000 cycles. The retained tensile properties obtained for the 2D and 3D PMCs are presented in Table 18. The results in Table 18 show that the pre-fatigued 3D PMC specimens at σ_{max} of 142.9 MPa and 192.6 MPa retained their stiffness. However, prior fatigue caused 10-23% reduction in tensile strength of the 3D PMC. In the case of the 2D PMC, the specimen retained 100% of its stiffness where it caused 50% reduction in tensile strength. The effect of prior tension-compression fatigue on the tensile stress-strain behavior of the 3D PMC and 2D PMC is shown in Figures 45 and 46, respectively. The tensile stress-strain curves obtained for the as-processed composites by Wilkinson [11] are included in Figures 45 and 46 for comparison. It is noteworthy that in all cases, the tensile stress-strain response of the pre-fatigued specimens remains nearly linear to failure.

Table 18: Retained properties of the 3D and 2D PMC with 0/90 fiber orientation specimens achieved fatigue run-out at elevated temperature.

Specimen #	Fatigue stress (Mpa)	Retained Modulus (GPa)	Modulus Retention (%)	Retained UTS (MPa)	Strength Retention (%)	Retained Failure Strain (%)
3D PMC with 0/90°						
C3-5	142.9	39.0	> 100	580.7	76.8	1.638^{NF}
C3-6	198.9	29.0	76.1	698.0	92.3	3.636
C3-7	192.6	36.6	95.4	682.4	90.3	1.472^{NF}
2D PMC with 0/90°						
C1-7	161.5	46.3	> 100	414.2	50.4	1.015^{NF}

^{NF}: Specimen did not fail during test. Test failed.

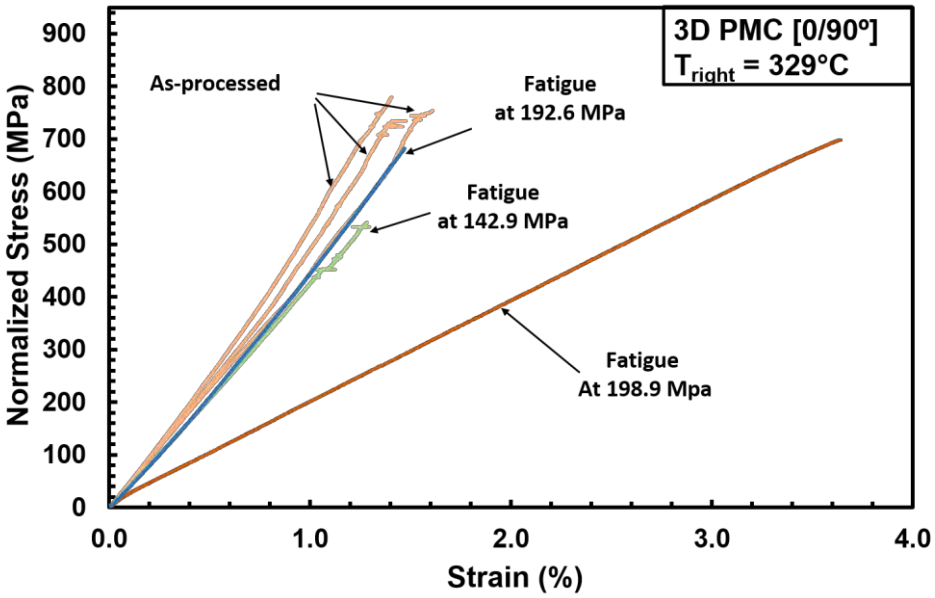

Figure 45: Effect of prior tension-compression fatigue on tensile stress-strain behavior of the 3D PMC with 0/90 fiber orientation at elevated temperature. As-processed results from Wilkinson [11].

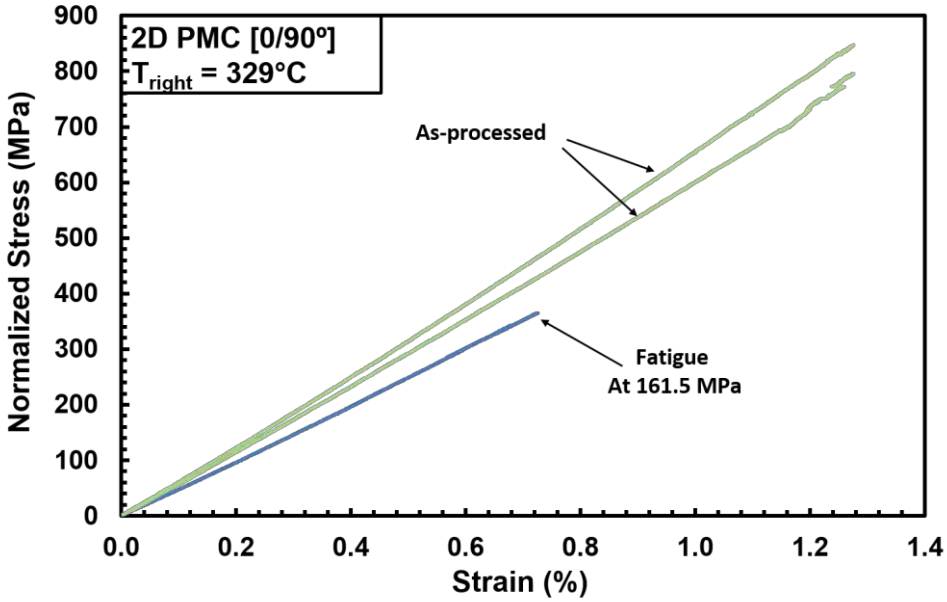

Figure 46: Effect of prior tension-compression fatigue on tensile stress-strain behavior of the 2D PMC with 0/90 fiber orientation at elevated temperature. As-processed results from Wilkinson [11].

5.6 Optical Microscopy Examination.

Zeiss optical microscopy was used to examine all the specimens tested in this research. Also, one as-processed specimen from each material system was examined. Those optical micrographs were used to study the failure mechanism of each material system.

5.6.1 Examination of the 3D PMC specimens with 0/90 fiber orientation.

Figure 47 shows the sides of the gage section of as-processed 3D PMC with 0/90˚ fiber orientation specimen. The optical micrographs reveal the through-thickness Z-fibers as well as the rugged texture of the specimen surface and matrix voids.

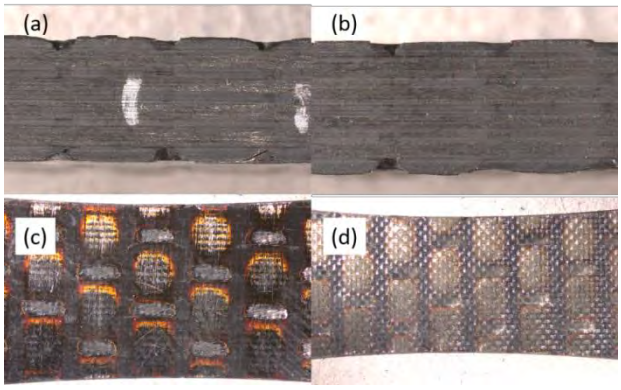

Figure 47: Optical micrographs of as-processed 3D PMC specimen with 0/90 fiber orientation (C3-9): (a) Front, (b) back, (c) left, (d) right.

The failure of the 3D PMC with 0/90˚ fiber orientation tested in tension-compression fatigue at σ_{max} of 212 MPa is shown in Figures 48 and 49. The failure occurred during compression portion of the loading cycle along the plane inclined at a 45˚ angle to the loading direction. Multiple matrix cracks are clearly visible. While initial ply delamination is apparent, the nearly intact through-thickness Z-fibers prevented complete delamination of the composite.

Figure 48: Stitched optical micrographs of the 3D PMC 0/90 specimen C3-10 after failure under tension-compression fatigue at σ_{max} of 211.8 MPa: (a) front (b) back

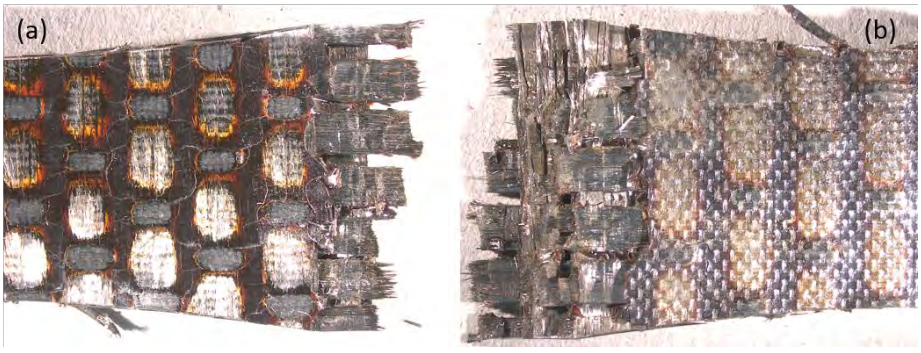

Figure 49: Optical micrograph of the 3D PMC 0/90˚ specimen C3-10 after failure under tension-compression fatigue at σ_{max} of 211.8 MPa: (a) left (b) right

Figures 50 and 51 show the failure of the 3D PMC specimen with 0/90˚ fiber orientation subjected to tension-to-failure test after surviving $2x10^5$ cycles of tension-compression fatigue at σ_{max} of 198.9 MPa. Warp fiber pullout and numerous matrix cracks are clearly visible with no evidence of delamination. More optical Micrographs of the 3D PMC provided in Appendix B.

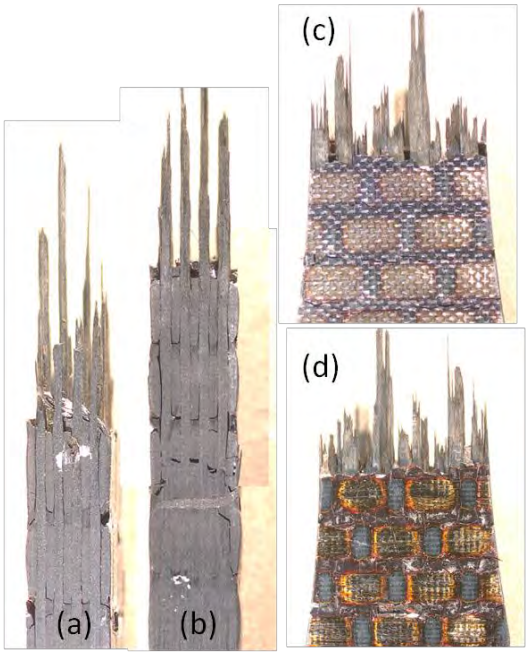

Figure 50: Stitched optical micrographs of the 3D PMC 0/90˚ specimen C3-6 failed in tension test after achieving fatigue run-out at σ_{max} of 199 MPa: (a) front (b) back (c) right (d) left

Figure 51: Optical micrograph of the 3D PMC 0/90˚ specimen C3-6 failed in tension test after achieving fatigue run-out at σ_{max} of 199 MPa.

5.6.2 Examination of the 2D PMC specimens with 0/90 fiber orientation.

Figure 52 shows the gage section of as-processed 2D PMC specimen C1-11 with 0/90˚ fiber orientation. In contrast to the 3D PMC, the surface of the 2D PMC specimen appears to be smooth and free of any voids or defects.

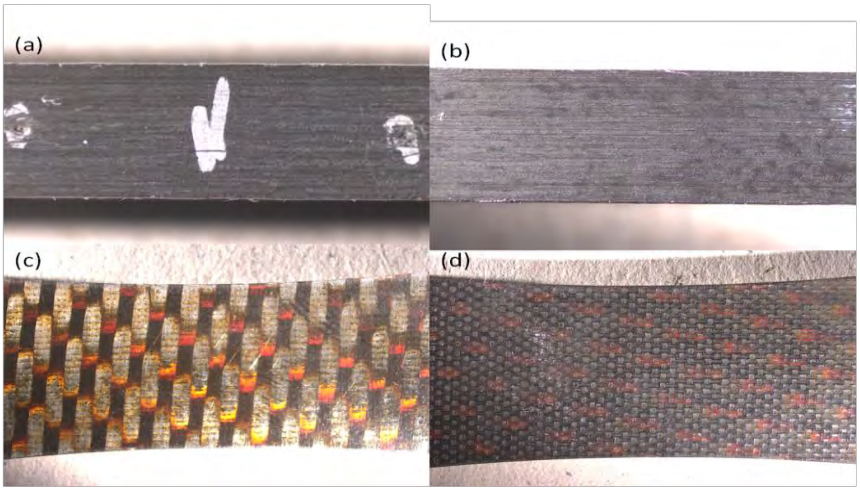

Figure 52: Optical micrograph of as-processed 2D PMC specimen with 0/90 fiber orientation C1-11: (a) Front, (b) back, (c) left, (d) right

The failure of the 2D PMC with 0/90˚ fiber orientation tested in tension-compression fatigue of σ_{max} of 238 MPa and 194 MPa are shown in Figures 53 and 54, respectively. The failure occurred during compression portion of the loading cycle along the plane inclined at a 45˚ angle to the loading direction. Considerable ply delamination is apparent. Interlaminar cracks extend to the gripping sections of the specimen. Recall that in the case of the 3D PMC, the through-thickness Z-fibers restricted complete ply delamination. More optical Micrographs of the 2D PMC provided in Appendix B.

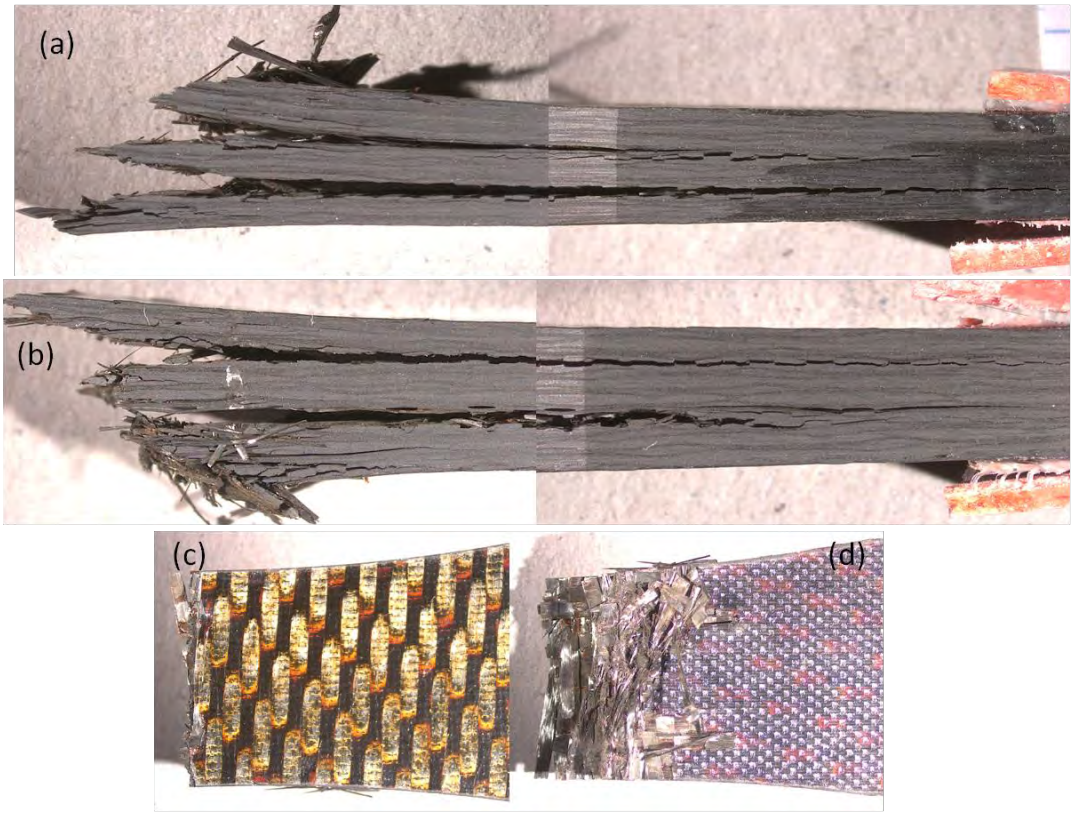

Figure 53: Stitched optical micrograph of the 2D PMC 0/90˚ specimen C1-8 after failure under tension-compression fatigue at σ_{max} of 238 MPa: (a) back (b) front (c) left (d) right.

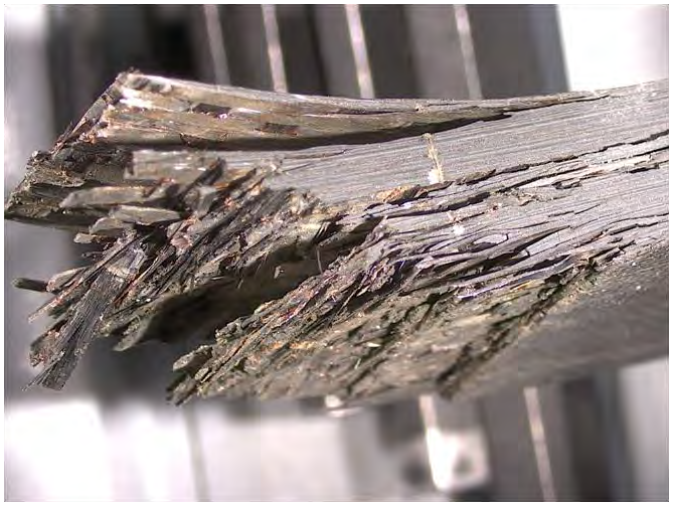

Figure 54: Optical micrograph of the 2D PMC 0/90˚ specimen C1-10 after failure under tension-compression fatigue at σ_{max} of 194 MPa.

VI. Conclusion and Recommendations

6.1 Conclusion

This research effort examined the compressive stress-strain and compressive properties of the 3D and 2D PMCs with 0/90˚ fiber orientation at room and elevated temperature. These results were compared to the tensile results obtained in Wilkinson work [10]. As expected, the 2D PMC showed higher compressive strength and modulus than the 3D PMC. For a given material system, compressive strength and compressive modulus were lower than the tensile strength and tensile modulus obtained in prior work [11]. For the two material systems, the increase in temperature had little effect on the compressive properties of both composites. In the case of the 3D PMC, the temperature increase resulted in a 17% loss of compressive modulus and a 15% loss of compressive strength. In the case of the 2D PMC, the temperature increase caused a 12% loss of compressive modulus and a 35% loss of compressive strength.

The tension-compression fatigue performance of the two material systems was investigated at elevated temperature. The 3D PMC showed a higher fatigue limit than the 2D PMC, but the 2D PMC exhibited a better fatigue performance at higher stress level. As expected, the 3D PMC specimens tested in fatigue exhibited had a localized failure, where ply delamination was restricted by through-thickness Z-fibers. In contrast, the 2D PMC specimens failed in fatigue showed severe ply delamination with interlaminar cracks extending from the failure location to the grip section.

6.2 Recommendations

Additional investigation research should be carried out to better comprehend the mechanical behavior of these 3D and 2D PMCs:

- Failure initiation and progression during compression and tension-compression fatigue loading.
- Different Loading rate of tension-compression fatigue tests.
- Higher temperature conditions should be investigated, since the results in this research and Wilkinson [11] showed no difference in the mechanical behavior between room temperature and elevated temperature where $T_{right} = 329^{\circ}C$.
- Compressive properties and tension-compression fatigue performance of the 3D and the 2D PMCs with ±45˚.

Appendix A: Additional Fatigue Plots

The compressive S-N curves for the 3D and 2D PMC with 0/90˚ fiber orientation in Figures 55 – 56 compares the fatigue performance of these material systems at the actual and normalized fatigue stresses.

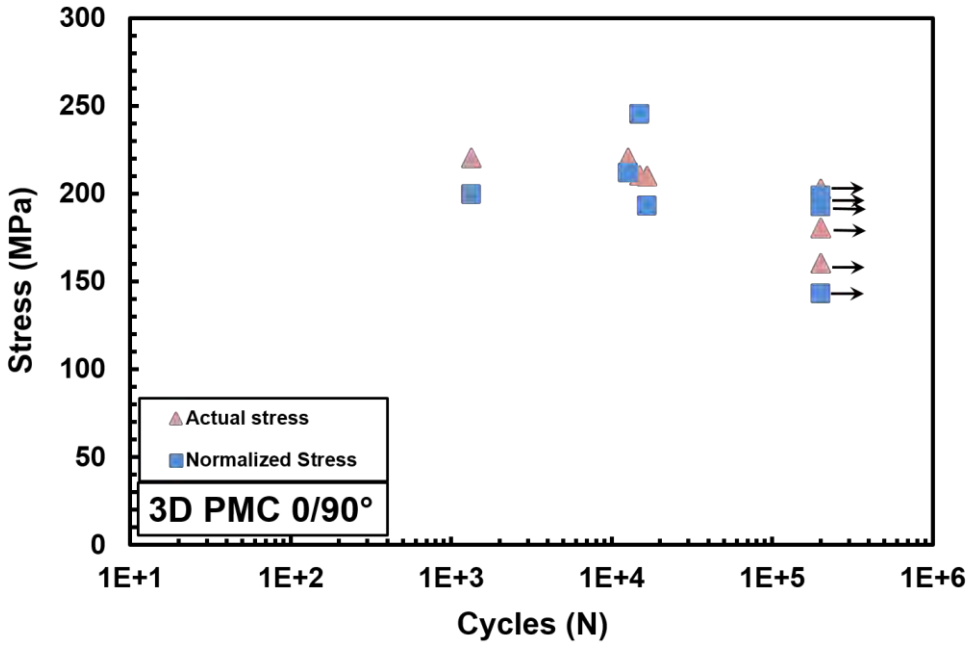

Figure 55: S-N curves obtained for the 3D PMC with the 0/90˚ fiber orientation at actual and normalized stresses. Arrows indicates fatigue run-out was achieved.

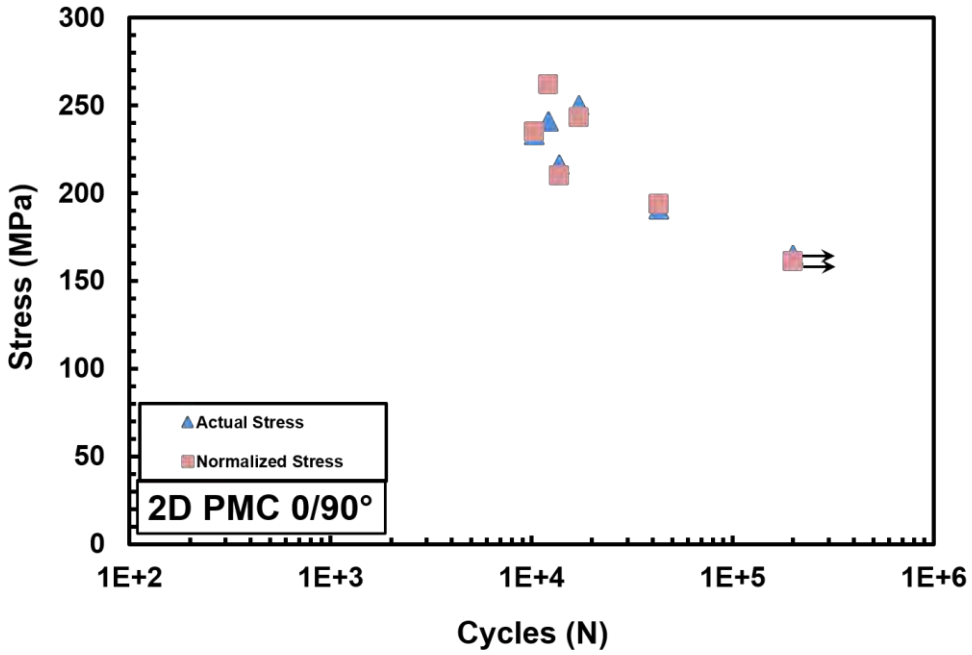

Figure 56: S-N curves obtained for the 2D PMC with the 0/90˚ fiber orientation at actual and normalized stresses. Arrows indicates fatigue run-out was achieved.

Figures 57 – 61 shows the stress-strain response for all the remaining 3D PMC specimens.

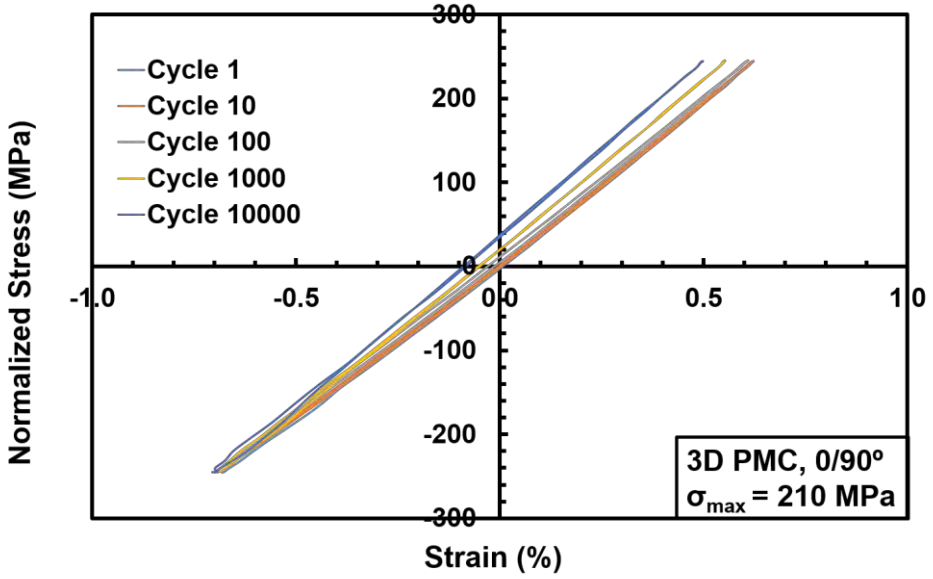

Figure 57: Evolution of stress-strain hysteresis response with fatigue cycles for specimen C3-1 of the 3D PMC with 0/90° fiber orientation at elevated temperature.

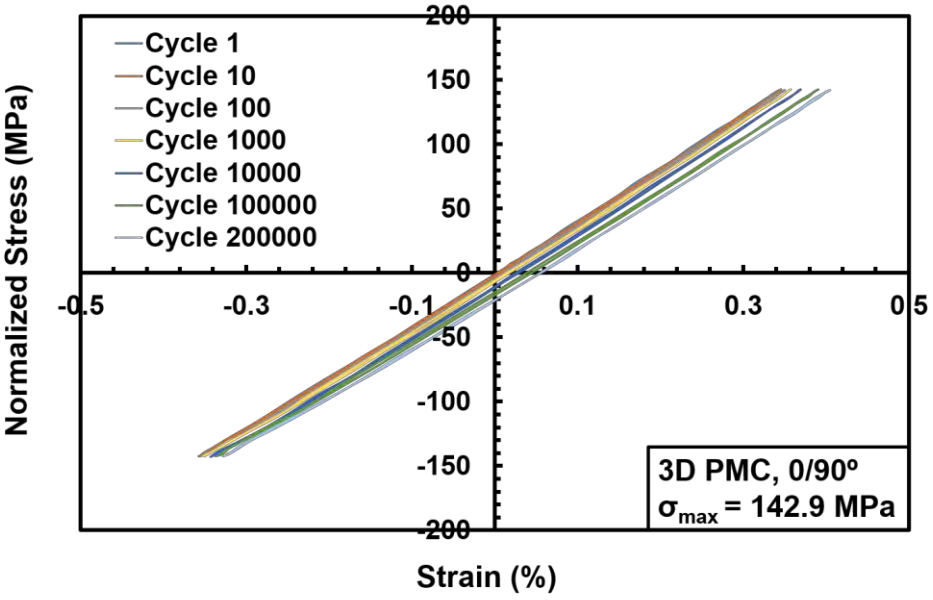

Figure 58: Evolution of stress-strain hysteresis response with fatigue cycles for specimen C3-5 of the 3D PMC with 0/90° fiber orientation at elevated temperature.

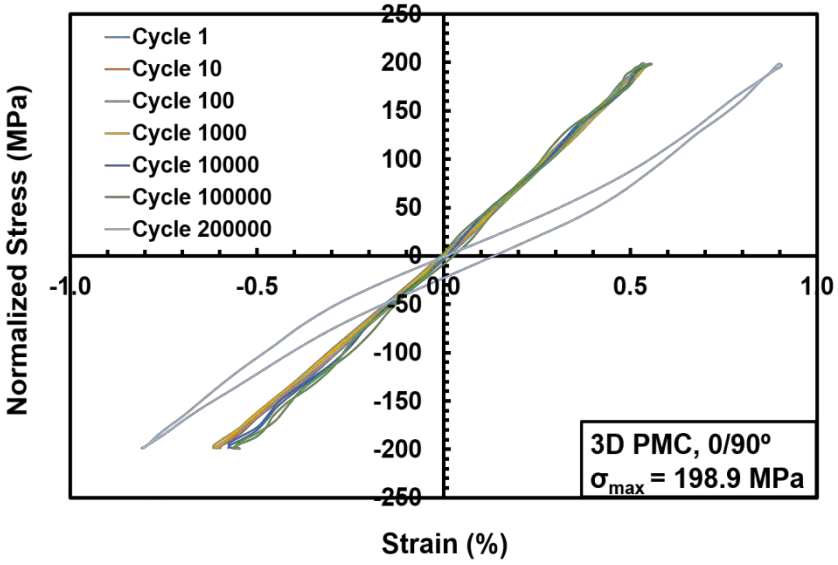

Figure 59: Evolution of stress-strain hysteresis response with fatigue cycles for specimen C3-6 of the 3D PMC with 0/90° fiber orientation at elevated temperature.

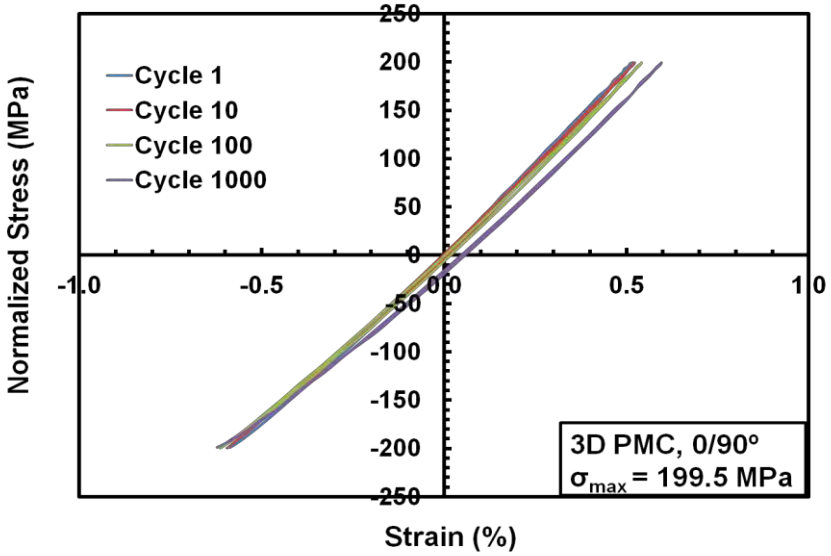

Figure 60: Evolution of stress-strain hysteresis response with fatigue cycles for specimen C3-8 of the 3D PMC with 0/90° fiber orientation at elevated temperature.

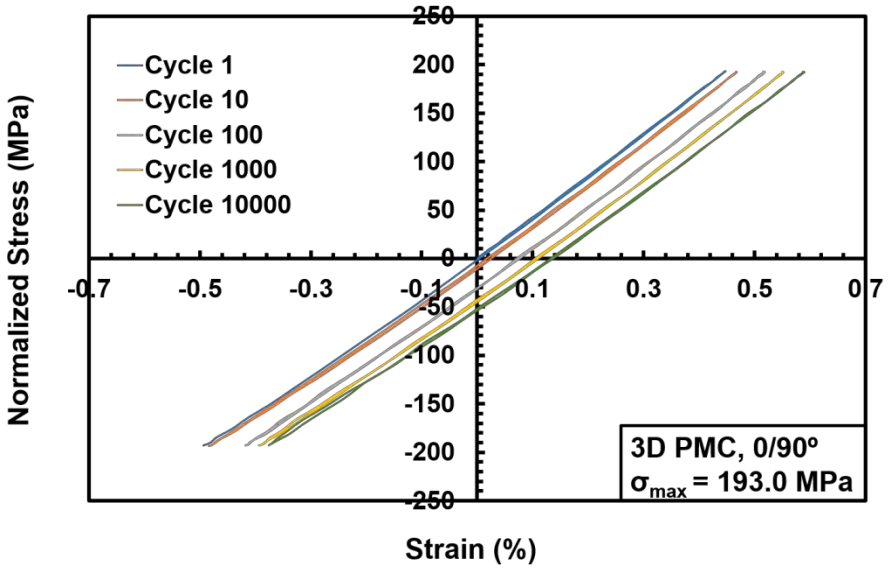

Figure 61: Evolution of stress-strain hysteresis response with fatigue cycles for specimen C3-9 of the 3D PMC with 0/90° fiber orientation at elevated temperature.

Figures 62 – 66 shows the stress-strain response for all the remaining 2D PMC specimens.

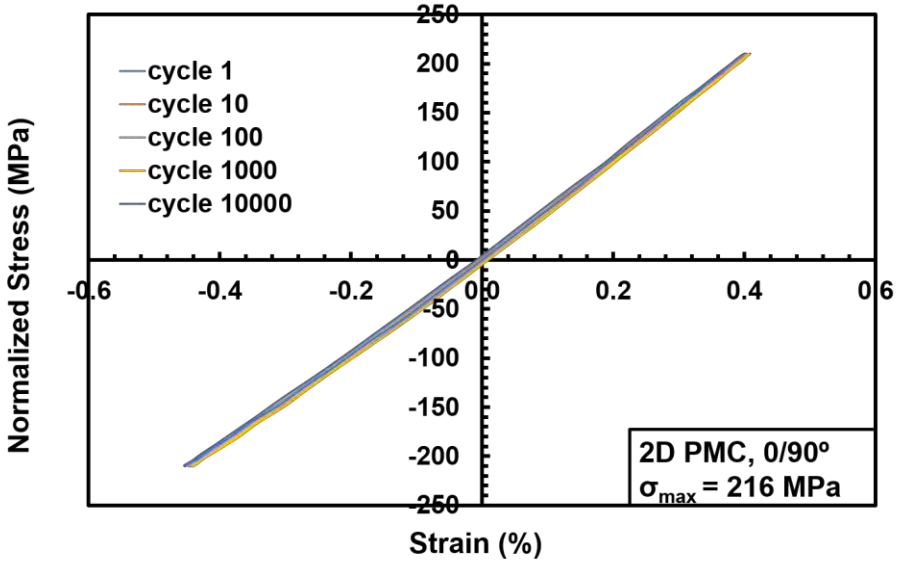

Figure 62: Evolution of stress-strain hysteresis response with fatigue cycles for specimen C1-6 of the 2D PMC with 0/90° fiber orientation at elevated temperature.

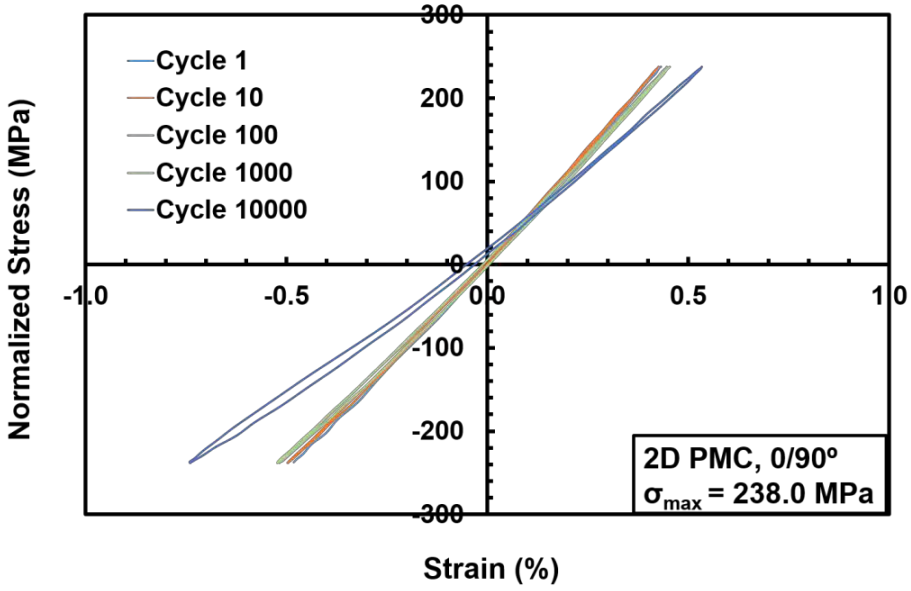

Figure 63: Evolution of stress-strain hysteresis response with fatigue cycles for specimen C1-8 of the 2D PMC with 0/90° fiber orientation at elevated temperature.

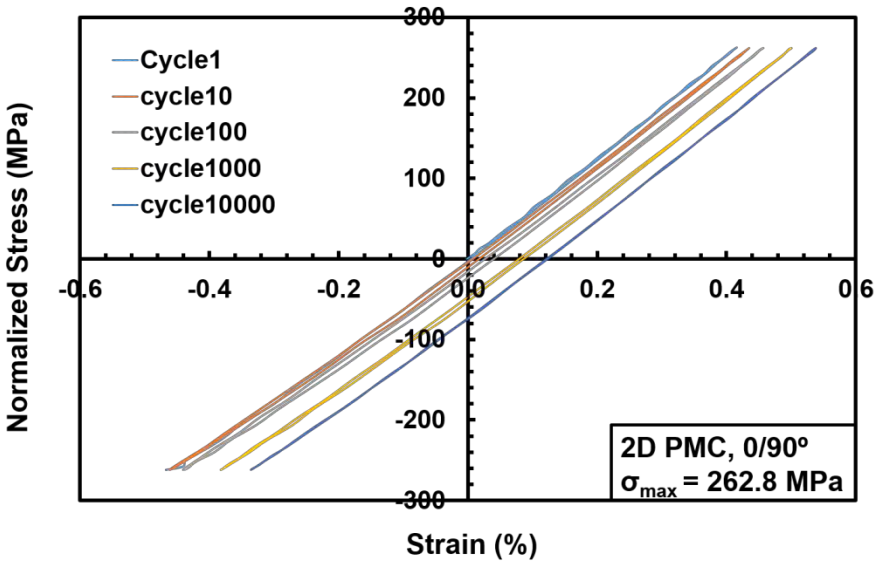

Figure 64: Evolution of stress-strain hysteresis response with fatigue cycles for specimen C1-9 of the 2D PMC with 0/90° fiber orientation at elevated temperature.

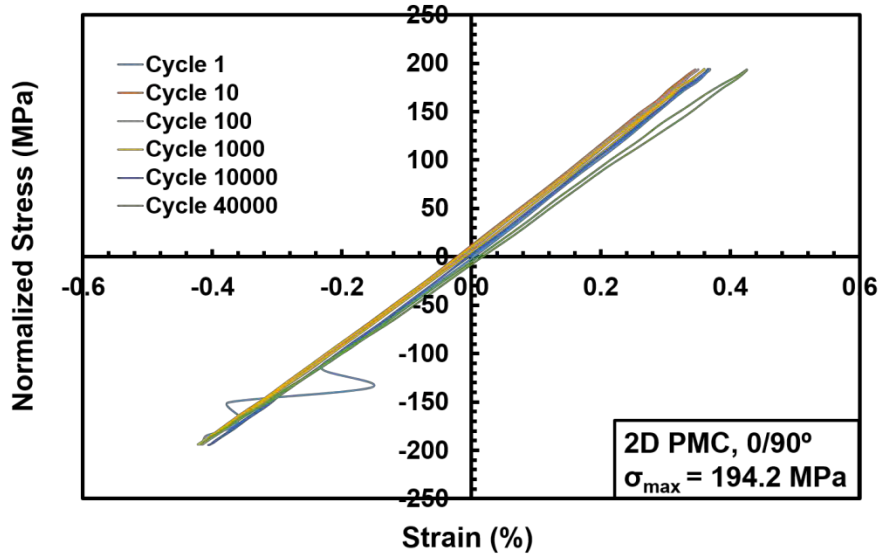

Figure 65: Evolution of stress-strain hysteresis response with fatigue cycles for specimen C1-10 of the 2D PMC with 0/90° fiber orientation at elevated temperature.

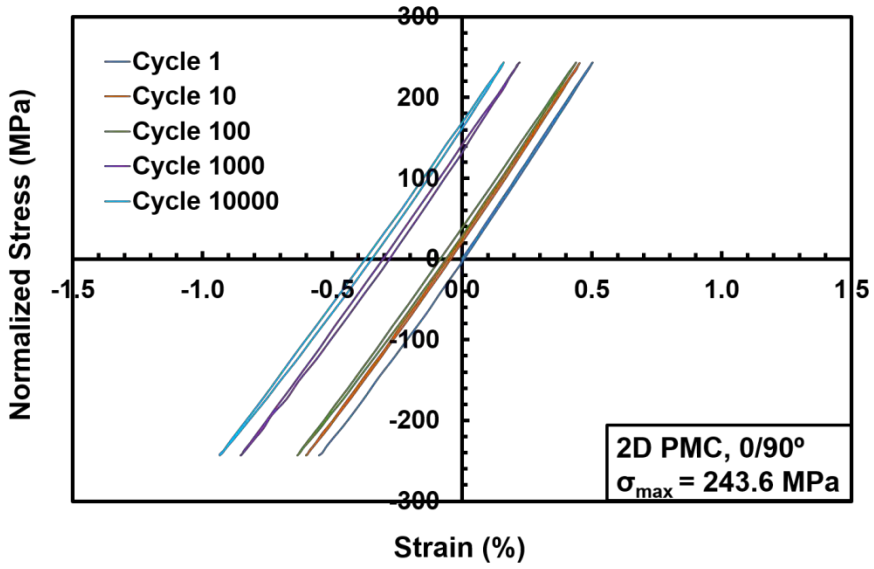

Figure 66: Evolution of stress-strain hysteresis response with fatigue cycles for specimen C1-11 of the 2D PMC with 0/90° fiber orientation at elevated temperature.

Appendix B: Additional Optical images.

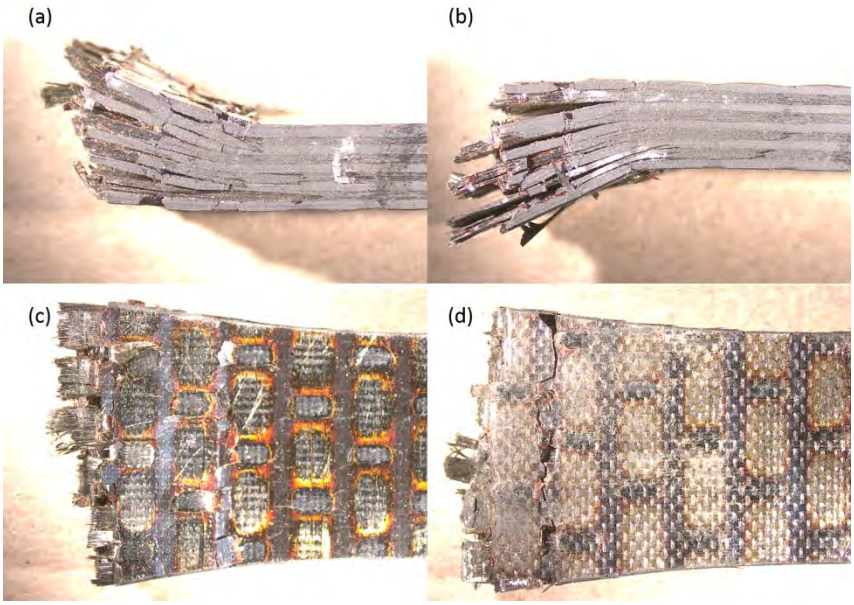

Figure 67: Optical micrographs of the 3D PMC 0/90 specimen C3-1 after failure under tension-compression fatigue at σ_{max} of 245 MPa: (a) front (b) back (c) left (d) right

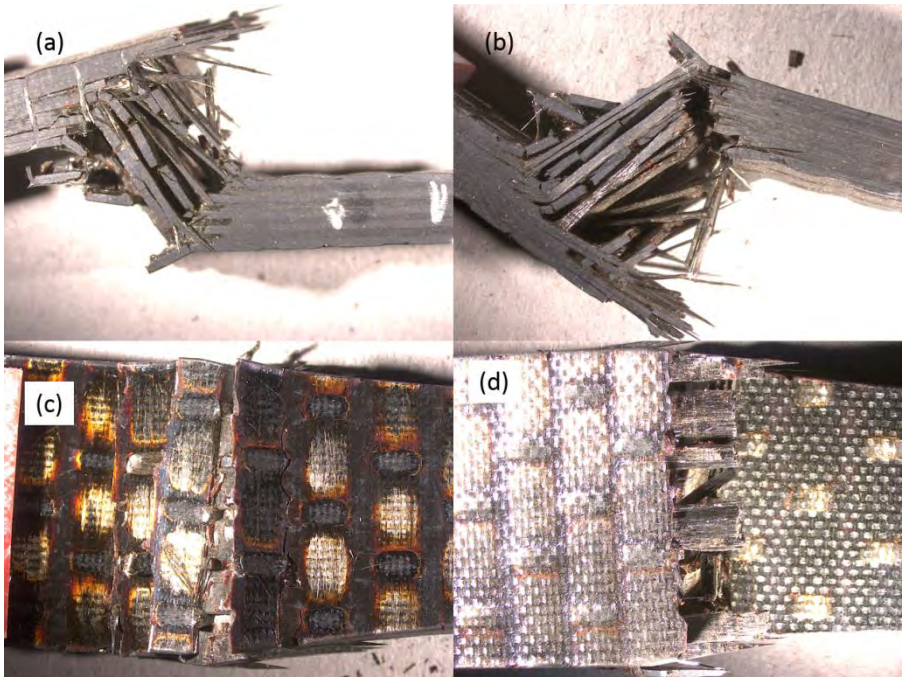

Figure 68: Optical micrographs of the 3D PMC 0/90 specimen C3-2 after failure under monotonic compression at room temperature: (a) front (b) back (c) left (d) right

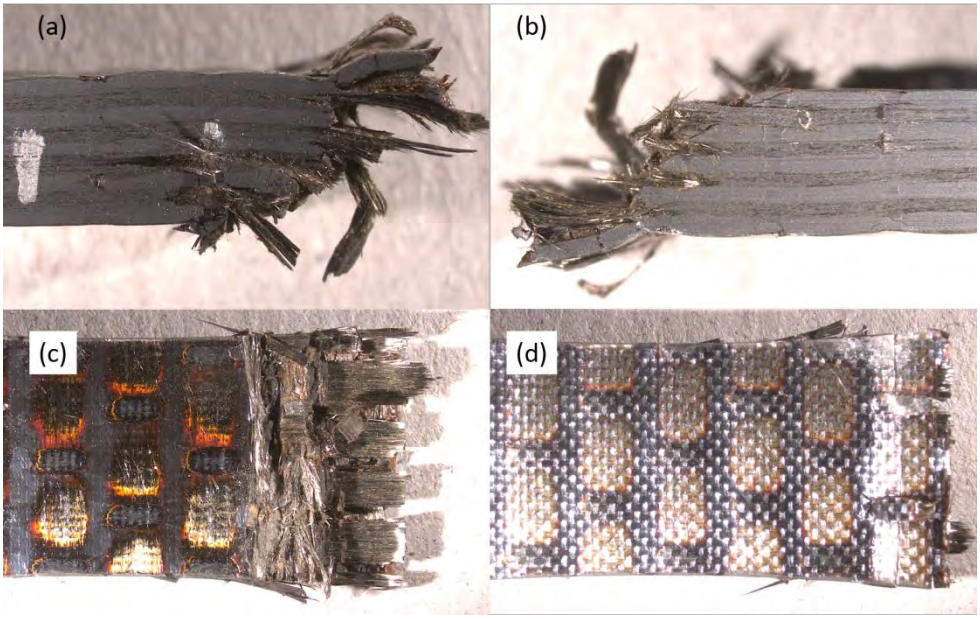

Figure 69: Optical micrographs of the 3D PMC 0/90 specimen C3-3 after failure under monotonic compression at elevated temperature: (a) front (b) back (c) left (d) right

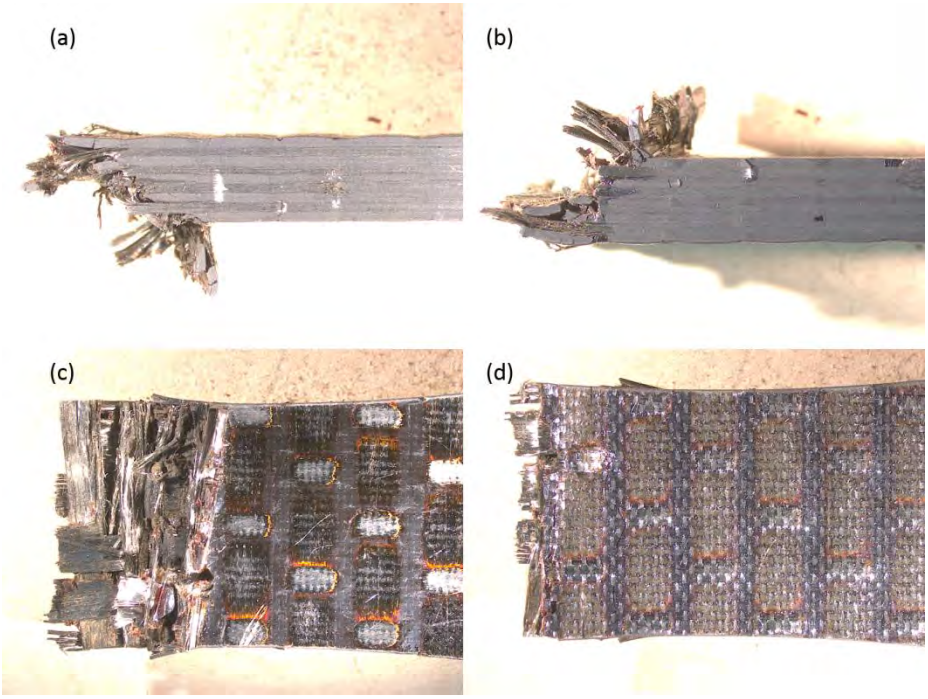

Figure 70: Optical micrographs of the 3D PMC 0/90 specimen C3-4 after failure under monotonic compression at elevated temperature: (a) front (b) back (c) left (d) right

Figures 71 – 72 shows the optical micrographs for the 3D PMC with 0/90º fiber orientation specimens C3-5 and C3-7 respectively. Both specimen achieved fatigue run-out of $2x10^5$ cycles. Tension-to-failure tests were conducted on the specimens, but both tests failed due to specimen failure at the grip section.

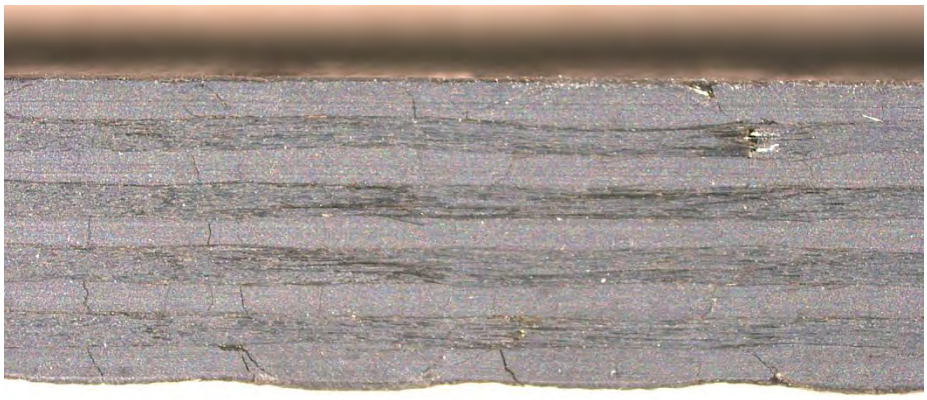

Figure 71: Optical micrograph of the 3D PMC 0/90 specimen C3-5 showing cracks on the specimen matrix. Specimen survived tension-compression fatigue at σ_{max} of 143 MPa.

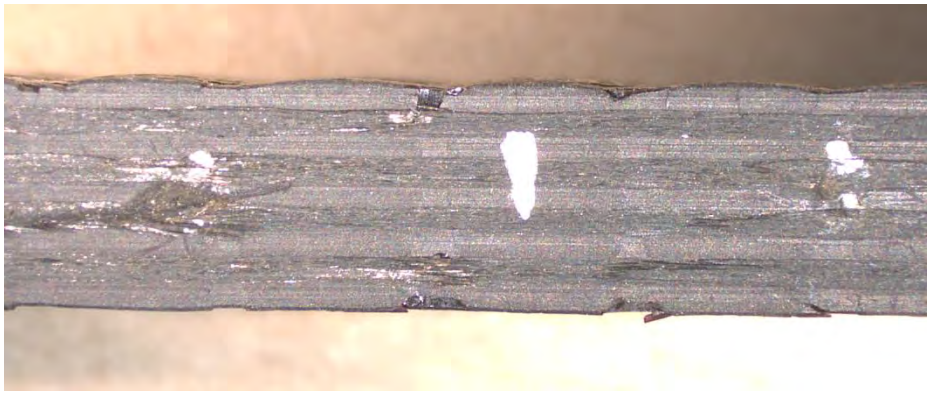

Figure 72: Optical micrograph of the 3D PMC 0/90 specimen C3-7 showing cracks and gauges on the specimen matrix. Specimen survived tension-compression fatigue at σ_{max} of 193 MPa.

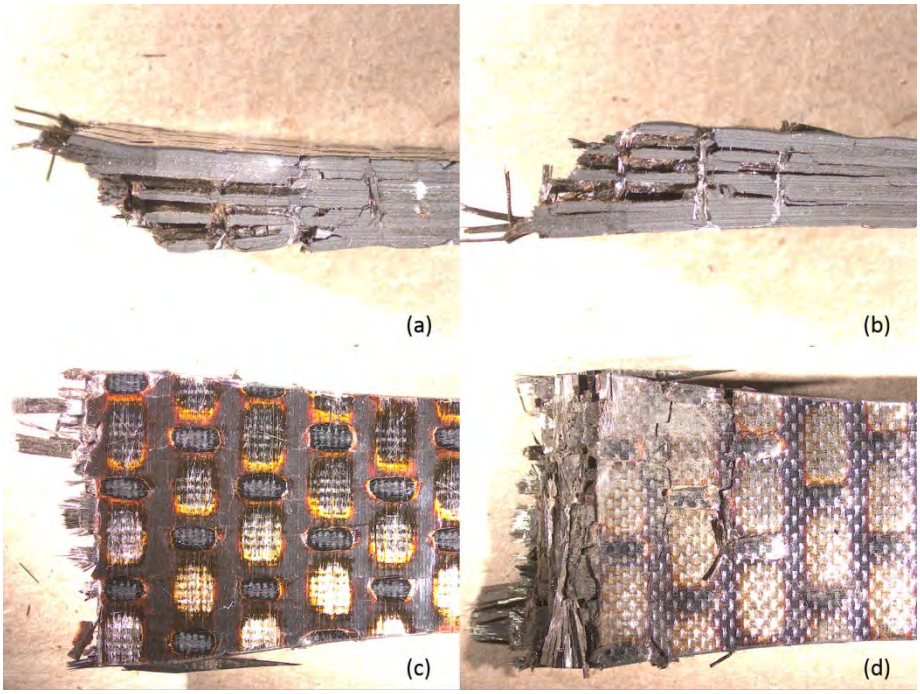

Figure 73: Optical micrographs of the 3D PMC 0/90 specimen C3-9 after failure under tension-compression fatigue at σmax of 193 MPa: (a) front (b) back (c) left (d) right

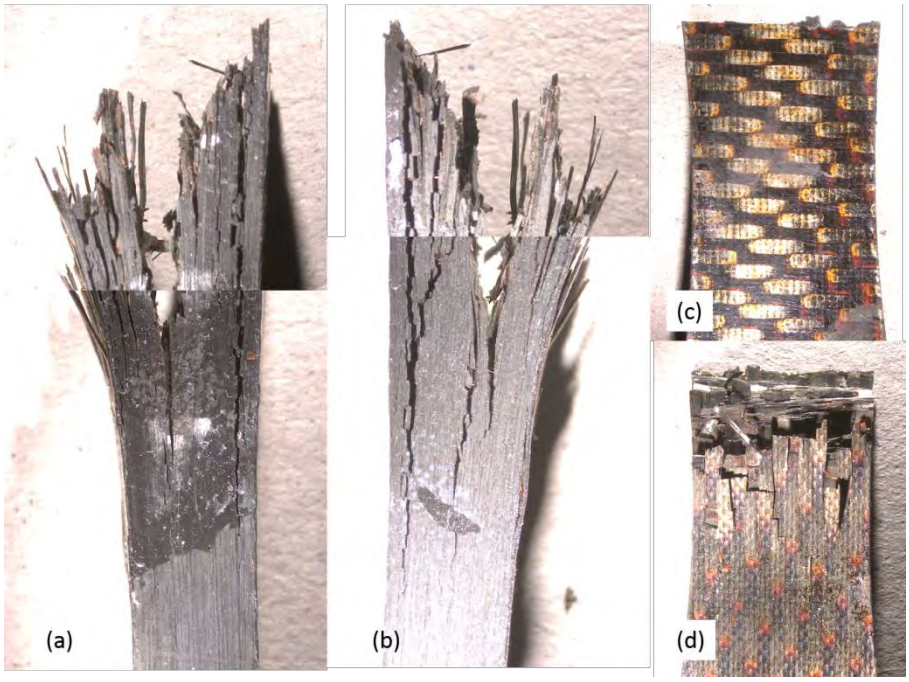

Figure 74: Stitched optical micrographs of the 2D PMC 0/90 specimen C1-3 after failure under monotonic compression at room temperature: (a) front (b) back (c) left (d) right

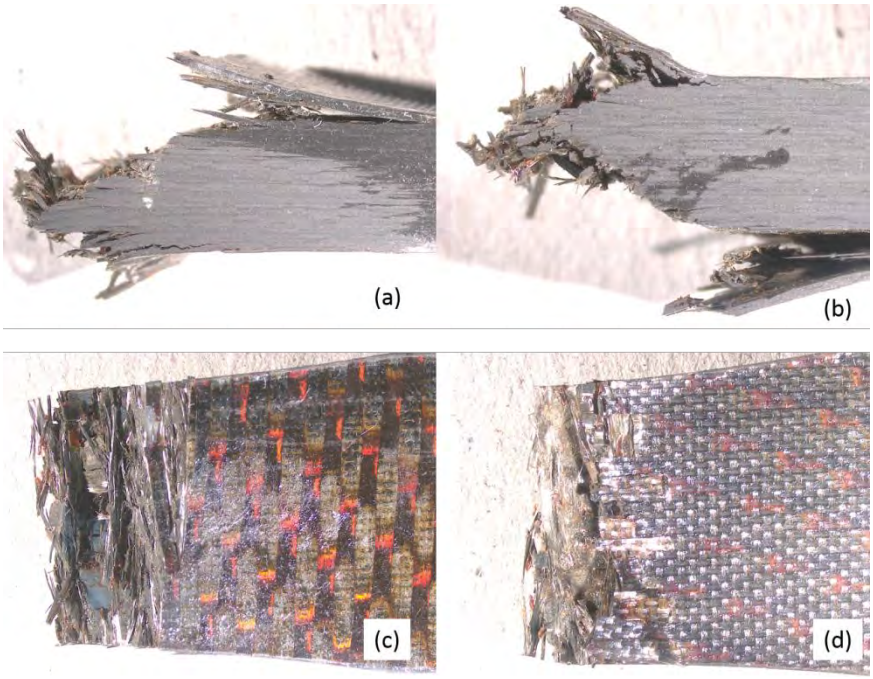

Figure 75: Optical micrographs of the 2D PMC 0/90 specimen C1-4 after failure under monotonic compression at elevated temperature: (a) front (b) back (c) left (d) right

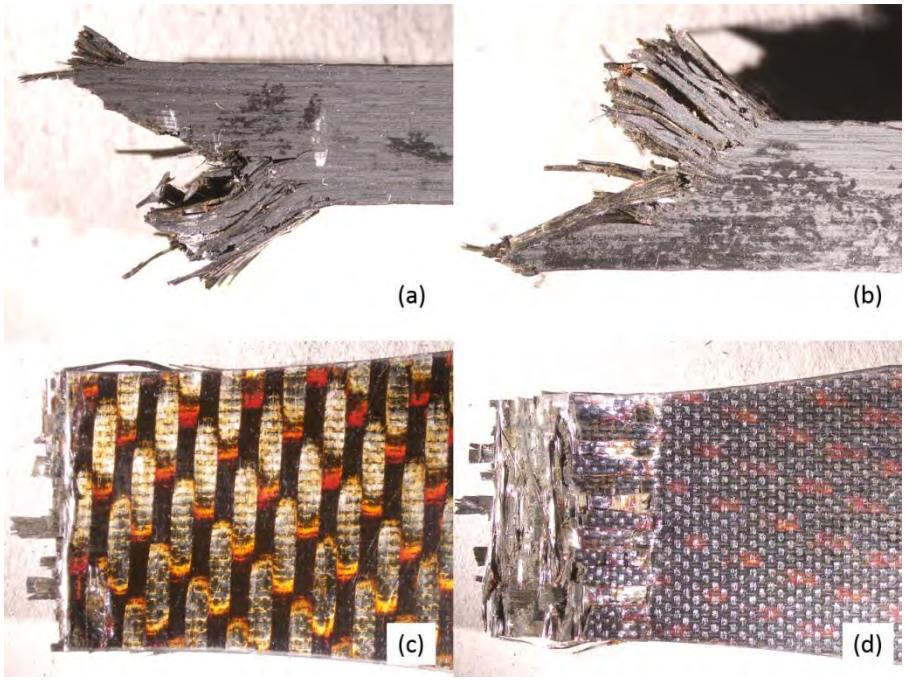

Figure 76: Optical micrographs of the 2D PMC 0/90 specimen C1-5 after failure under monotonic compression at elevated temperature: (a) front (b) back (c) left (d) right

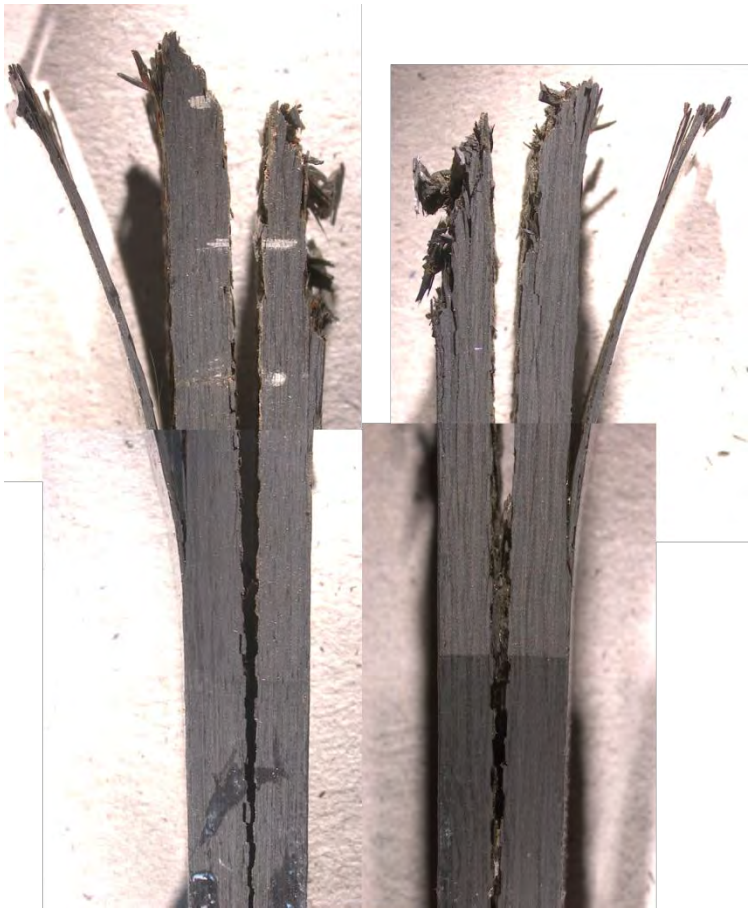

Figure 77: Stitched optical micrographs of the 2D PMC 0/90 specimen C1-6 after failure under tension-compression fatigue at σ_{max} of 211 MPa. From left to right: front, back

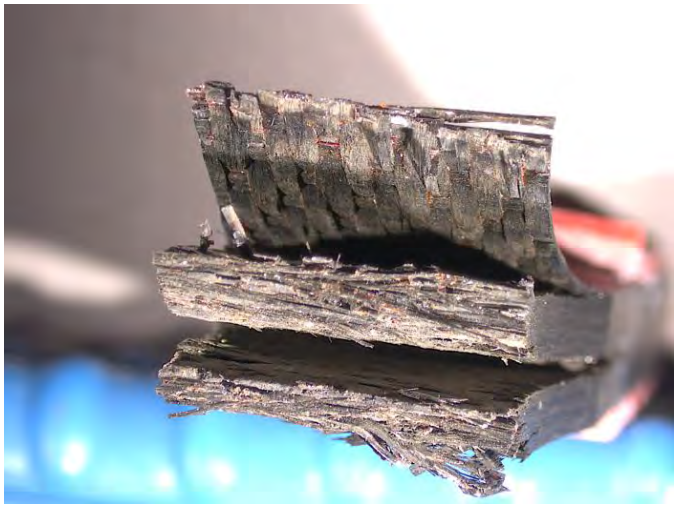

Figure 78: Optical micrographs of the 2D PMC 0/90˚ specimen C1-6 after failure under tension-compression fatigue at σmax of 211 MPa viewed from an angle

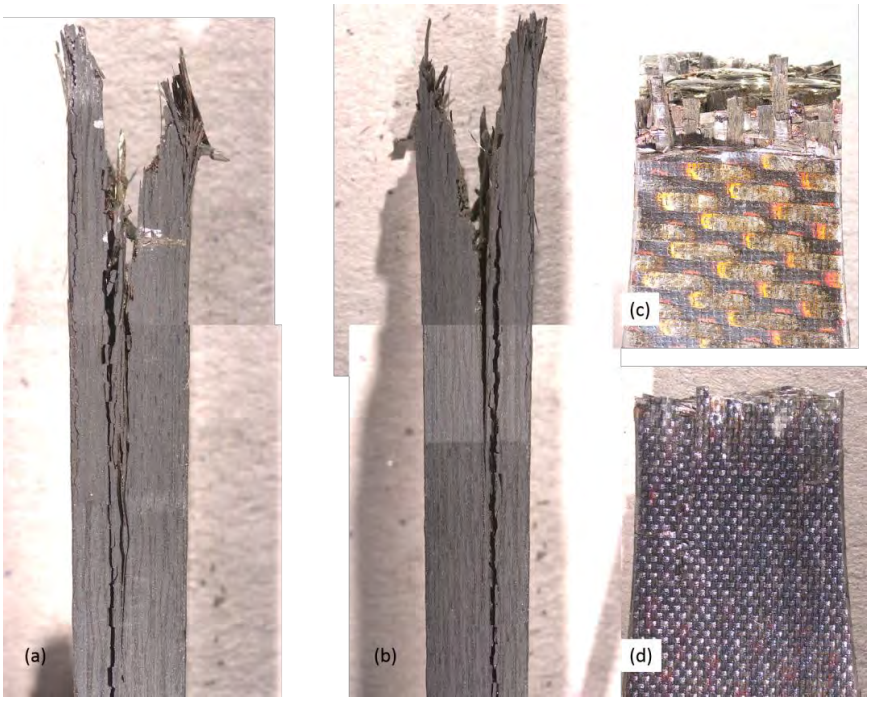

Figure 79: Stitched optical micrographs of the 2D PMC 0/90 specimen C1-9 after failure under tension-compression fatigue at σ_{max} of 262.2 MPa: (a) front (b) back (c) left (d) right

Bibliography

1. Carvelli, V., Gramellini, G., Lomov, S. V., Bogdanovich, A. E., Mungalov, D. D., and Verpoest, I. "Fatigue behavior of non-crimp 3D orthogonal weave and multi-layer plain weave E-glass reinforced composites". Composites Science and Technology, 70 (14): 2068 – 2076, 2010. ISSN 0266-3538.

2. Chawla, K. K. Ceramic Matrix Composites. Kluwer Academic Publishers, Norwell,MA, 2nd edition, 2003.

3. Daniel, Isaac M. and Ori Ishai. "Engineering Mechanics of Composite Materials". Oxford University Press, New York, NY, 2nd edition, 1994.

4. F.C. Campbell. "Structural Composite Materials" ASM International®, Materials Park, Ohio 44073-0002, www.asminternational.org.

5. Federal Aviation Administration. "Aviation Maintenance Technician Handbook". http://www.faa.gov/regulations policies/handbooks manuals/aircraft/ amt airframe handbook/, 2012. [Online; accessed 9 Sep 2013].

6. Jones, John. "Polyimide Boosts High-Temperature Performance". http://spino_.nasa.gov/Spino_2008/ip 5.html, May 2011. [Online; accessed 2 Sep 2013].

7. J.M. Corum et al., Durability-Based Design Properties of Reference Crossply Carbon-Fiber Composite, ORNL/TM-200/322, Oak Ridge National Laboratory, Oak Ridge,

8. Jones, Tyler. "Tension-Compression Fatigue of Hi-Nicalon/SiC Ceramic Matrix Composite at 1200°C in Air and in Steam". Master's thesis, Air Force Institute of Technology, Wright-Patterson AFB, Ohio, 2011.

9. Lincoln, Jason E. "NRPE Composite Materials". http://www.p2si.com/prepregs/datasheets/NRPE-Public-Release.pdf.

10. Martin, Rick and Daniel Evans. "Reducing Costs in Aircraft: The Metals a_ordability Initiative Consortium". Journal of the Minerals, Metals, and materials Society, 42(3):24–28, 2000.

11. Wilkinson, M. “Mechanical Properties and Fatigue Behavior of Unitized Composite Airframe Structures at Elevated Temperature”. Master’s thesis, Air Force Institute of Technology, Wright-Patterson AFB, Ohio, 2013.

12. Robert, M. “Mechanics of Composite Materials”. CRC Press, second Edition, ISBN-10: 156032712x, July 1998.

13. Ruggles-Wrenn, M. B., D. T. Christensen, A. L. Chamberlain, J. E. Lane, and T. S. Cook. “E_ect of frequency and environment on fatigue behavior of a fCVIg SiC/SiCceramic matrix composite at 1200°C”. Composites Science and Technology, 71(2):190 – 196, 2011. ISSN 0266-3538.

14. Schetz, Joseph A., Alan Baker, Stuart Dutton, and Donald Kelly. “Composite Materials for Aircraft Structures”. AIAA, Reston, VA, 2nd edition, 2004.

15. Stig, Fredrik. “3D-Woven Reinforcement in Composites”. Ph.D. thesis, KTH School of Engineering Sciences, Stockholm, Sweden, 2012.

16. U.S Congress, Office of Technology Assessment, Advanced Materials by Design, OTA-E-351 (Washington, DC: U.S. Government Printing Office, June 1988).

REPORT DOCUMENTATION PAGE

Form Approved
OMB No. 074-0188

1. REPORT DATE *(DD-MM-YYYY)*	2. REPORT TYPE	3. DATES COVERED *(From – To)*
21-08-2015	Master's Thesis	October 2013 – September 2015

TITLE AND SUBTITLE

Tension-Compression Fatigue Behavior of
2D and 3D Polymer Matrix Composites
at Elevated Temperature

5a. CONTRACT NUMBER

5b. GRANT NUMBER

5c. PROGRAM ELEMENT NUMBER

6. AUTHOR(S)

Alnatifat, Saleh A., Captain, RSAF

5d. PROJECT NUMBER

5e. TASK NUMBER

5f. WORK UNIT NUMBER

7. PERFORMING ORGANIZATION NAMES(S) AND ADDRESS(S)
Air Force Institute of Technology
Graduate School of Engineering and Management (AFIT/ENY)
2950 Hobson Way, Building 640
WPAFB OH 45433-8865

8. PERFORMING ORGANIZATION REPORT NUMBER

AFIT-ENY-15-S-052

9. SPONSORING/MONITORING AGENCY NAME(S) AND ADDRESS(ES)
Air Force Research Laboratory/RQVS
Mr. Michael Falugi
2790 D Street, Bldg. 65
WPAFB OH 45433-7402
(937) 656-8810 michael.falugi@us.af.mil

10. SPONSOR/MONITOR'S ACRONYM(S)

AFRL/RQVS

11. SPONSOR/MONITOR'S REPORT NUMBER(S)

12. DISTRIBUTION/AVAILABILITY STATEMENT
DISTRUBTION STATEMENT A**.** APPROVED FOR PUBLIC RELEASE; DISTRIBUTION UNLIMITED.

13. SUPPLEMENTARY NOTES
This material is declared a work of the U.S. Government and is not subject to copyright protection in the United States.

14. ABSTRACT

In this Research effort, the tension-compression fatigue behavior of the 3D and 2D PMCs with 0/90˚ fiber orientation (newly developed) was investigated. These polymer composites consist of an NRPE (high-temperature polyimide) matrix with carbon fiber reinforcement. Compressive properties were assessed at (1) room temperature and (2) elevated temperature with one side, T_{right}, at 329˚C and the other side open to the ambient air. Tension-compression fatigue tests were conducted at elevated temperature with a frequency of 1 Hz and a ratio of minimum to maximum stress of -1.

15. SUBJECT TERMS
Polymer Matrix Composites, 3D Non-Crimp Orthogonal Weave, Fatigue, Mechanical Properties

16. SECURITY CLASSIFICATION OF:			17. LIMITATION OF ABSTRACT	18. NUMBER OF PAGES	19a. NAME OF RESPONSIBLE PERSON
a. REPORT	b. ABSTRACT	c. THIS PAGE			Dr. Marina B. Ruggles-Wrenn (ENY)
U	U	U	UU	104	19b. TELEPHONE NUMBER *(Include area code)* (937) 255-3636 x4641 marina.ruggles-wrenn@afit.edu

Standard Form 298 (Rev. 8-98)
Prescribed by ANSI Std. Z39-18